

1 **The Nedd4L ubiquitin ligase is activated by FCHO2-generated membrane
2 curvature**

3

4 Yasuhisa Sakamoto¹, Akiyoshi Uezu¹, Koji Kikuchi¹, Jangmi Kang², Eiko Fujii²,
5 Toshiro Moroishi³, Shiro Suetsugu⁴, and Hiroyuki Nakanishi^{1,2*}

6

7 ¹Department of Molecular Pharmacology, Faculty of Life Sciences, Kumamoto
8 University, 1–1–1 Honjyo, Kumamoto 860-8556, Japan

9 ²Faculty of Clinical Nutrition and Dietetics, Konan Women’s University, 6–2–23
10 Morikita-machi, Kobe 658-0001, Japan

11 ³Department of Molecular and Medical Pharmacology, Faculty of Life Sciences,
12 Kumamoto University, 1–1–1 Honjyo, Kumamoto 860-8556, Japan

13 ⁴Division of Biological Science, Graduate School of Science and Technology, Nara
14 Institute of Science and Technology, 8916-5 Takayama-cho, Ikoma 630-0192, Japan

15 *Corresponding author. Tel: +81-96-373-5074; Fax: +81-96-373-5078; E-mail:
16 hnakanis@gpo.kumamoto-u.ac.jp

17

18

19

1 **Abstract**

2

3 The C2-WW-HECT domain ubiquitin ligase Nedd4L regulates membrane sorting
4 during endocytosis through the ubiquitination of cargo molecules such as the epithelial
5 sodium channel (ENaC). Nedd4L is catalytically autoinhibited by an intramolecular
6 interaction between its C2 and HECT domains, but the protein's activation mechanism
7 is poorly understood. Here, we show that Nedd4L activation is linked to membrane
8 shape by FCHO2, a Bin-Amphiphysin-Rsv (BAR) domain protein that regulates
9 endocytosis. FCHO2 was required for the Nedd4L-mediated ubiquitination and
10 endocytosis of ENaC, with Nedd4L co-localizing with FCHO2 at clathrin-coated pits. In
11 cells, Nedd4L was specifically recruited to, and activated by, the FCHO2 BAR domain.
12 Furthermore, we reconstituted FCHO2-induced recruitment and activation of Nedd4L in
13 vitro. Both the recruitment and activation were mediated by membrane curvature rather
14 than protein-protein interactions. The Nedd4L C2 domain recognized a specific degree
15 of membrane curvature that was generated by the FCHO2 BAR domain, with this
16 curvature directly activating Nedd4L by relieving its autoinhibition. Thus, we show for
17 the first time a specific function (i.e., recruitment and activation of an enzyme
18 regulating cargo sorting) of membrane curvature by a BAR domain protein.

19

20 **Keywords:** Nedd4L; FCHO2; clathrin; endocytosis; membrane curvature.

21

1 **Introduction**

2

3 Posttranslational modification of proteins by covalent attachment of ubiquitin (Ub) is
4 catalyzed by three enzymes: a Ub-activating enzyme (E1), a Ub-conjugating enzyme
5 (E2), and a Ub-protein ligase (E3) that determines substrate specificity (Hershko &
6 Ciechanover, 1998). E3 Ub ligases are classified into two categories based on their Ub
7 transfer mechanisms: RING finger/U-box E3 and HECT-type E3. The Nedd4 family
8 belongs to HECT-type E3 Ub ligases and consists of nine members, including
9 Nedd4/Nedd4-1, Nedd4L/Nedd4-2, Itch, Smurf1, Smurf2, WWP1, WWP2, NEDL1,
10 and NEDL2 (Ingham *et al*, 2004; Rotin & Kumar, 2009). They are characterized by a
11 common modular organization, with an N-terminal C2 domain, two to four WW
12 domains, and a C-terminal catalytic HECT domain. While the C2 domain was originally
13 identified in protein kinase C (PKC) as a Ca^{2+} -dependent phosphatidylserine (PS)-
14 binding domain (Nishizuka, 1992), it shows significant diversity in the binding partners,
15 including intracellular proteins and other phospholipids, such as phosphatidylinositol
16 (4,5)-bisphosphate [PI(4,5)P₂] (Lemmon, 2008). The WW domains recognize proline-
17 rich motifs, such as PPxY (PY motif, where x is any residue), of substrates or adaptor
18 proteins. The HECT domain catalyzes the isopeptide bond formation between the Ub C
19 terminus and the substrate lysine residues. At least some of the Nedd4 family members,
20 including Nedd4L, are catalytically autoinhibited by an intramolecular interaction
21 between the C2 and HECT domains (Wang *et al*, 2010; Wiesner *et al*, 2007; Zhu *et al*,
22 2017). However, the activation mechanism of the Nedd4 family is poorly understood.

23 The Nedd4 family is implicated in a wide variety of cellular processes by

1 regulating membrane trafficking and degradation of components of various signaling
2 pathways (Ingham *et al*, 2004; Rotin & Kumar, 2009). Among a diversity of substrates,
3 the best-characterized is the epithelial sodium channel (ENaC). This channel is
4 composed of three subunits, α -, β -, and γ ENaC, each of which possesses two
5 transmembrane segments and intracellular N- and C-termini with a large extracellular
6 loop (Butterworth, 2010; Rotin & Staub, 2011; Rossier, 2014). Each subunit has a PY
7 motif at the cytosolic C-terminus. Nedd4L Ub ligase specifically binds to the PY motif
8 and mediates the ubiquitination of lysine residues on the N-terminus of at least α - and
9 γ ENaC at the plasma membrane. Ub serves as an internalization signal for recognition
10 by adaptor proteins, such as epsin and Eps15, for clathrin-mediated endocytosis (CME)
11 (Traub, 2009). Consequently, ENaC is constitutively internalized through CME.
12 Heterozygous mutations of the PY motif of β - or γ ENaC lead to impaired ubiquitination
13 and endocytosis, resulting in persistence of the channels at the cell surface and increased
14 Na^+ absorption in Liddle syndrome, an autosomal dominant form of severe
15 hypertension.

16 The process of CME begins at the cytoplasmic surface of the plasma
17 membrane with the assembly of clathrin with adaptor proteins and transmembrane cargo
18 molecules (Doherty & McMahon, 2009; Traub, 2009). In parallel with this assembly,
19 membrane curvature is generated to form hemispherical clathrin-coated pits (CCPs).
20 This process leads to deep membrane invaginations. Subsequently, the neck of
21 invaginated pits is constricted and severed to separate the newly formed clathrin-coated
22 vesicles (CCVs) from the plasma membrane. These membrane curvatures are
23 considered to be generated, sensed, and/or maintained by Bin-Amphiphysin-Rsv (BAR)

1 domain superfamily proteins. BAR domains form a crescent-shaped dimer characterized
2 by a specific degree of intrinsic curvature. They bind to negatively charged
3 phospholipids, such as PS, and force membranes to bend according to their intrinsic
4 curvatures, thereby inducing the formation of membrane tubules with specific diameters
5 (curvatures). For example, the diameters of membrane tubules generated by the
6 amphiphysin BAR domain, FCHO2 BAR domain, and FBP17 BAR domain are 20–50
7 nm (sharper curvature) (Peter *et al*, 2004; Takei *et al*, 1999; Yin *et al*, 2009), 50–80 nm
8 (intermediate curvature) (Henne *et al*, 2007), and ~150 nm (Takano *et al*, 2008)
9 (shallower curvature), respectively.

10 The FCHO2 BAR domain has been proposed to trigger the initial invagination
11 for CCP formation (Henne *et al*, 2010). FCHO2 binds to the flat surface of the plasma
12 membrane at sites where CCPs will form. FCHO2 then generates the initial membrane
13 curvature and recruits the clathrin machinery for CCP formation. Here, we report the
14 role of FCHO2 in Nedd4L-mediated ENaC endocytosis and show that FCHO2 BAR
15 domain-generated membrane curvature induces the recruitment and activation of
16 Nedd4L.

17

18 **Results**

19

20 **FCHO2 is required for Nedd4L-mediated ubiquitination and endocytosis of ENaC**
21 To study the role of FCHO2 in ENaC endocytosis, we established a HeLa cell line
22 stably expressing all three subunits, α -, β -, and γ ENaC ($\alpha\beta\gamma$ ENaC-HeLa cells) (Fig
23 EV1A-C). A FLAG tag was introduced into the extracellular region of α ENaC in a

1 position previously shown not to affect channel activity (Firsov *et al*, 1996). Upon
2 FCHO2 knockdown by small interfering RNA (siRNA) methods, ENaC internalization
3 was reduced, as was upon Nedd4L knockdown (Zhou *et al*, 2007) (Fig 1 A and B).
4 Transferrin receptor (TfR) internalization was reduced upon FCHO2 knockdown but not
5 upon Nedd4L knockdown (Fig 1C). The phenotype of FCHO2 knockdown in ENaC
6 internalization was rescued by an siRNA-resistant (sr) form of FCHO2 (Fig 1D and
7 Appendix Fig S1). Furthermore, α ENaC ubiquitination was reduced upon FCHO2 or
8 Nedd4L knockdown but not upon FBP17 knockdown (Fig 1E and Fig EV2). FCHO2 or
9 Nedd4L knockdown increased α ENaC expression at the cell surface (Fig 1E and F).
10 These results suggest that FCHO2 is required for Nedd4L-mediated ubiquitination and
11 endocytosis of ENaC.

12

13 **Recruitment and activation of Nedd4L by FCHO2 in cells**

14 Immunofluorescence microscopy revealed that in $\alpha\beta\gamma$ ENaC-HeLa cells, cell-surface
15 α ENaC co-localized with FCHO2 at clathrin-coated structures (Fig 2A). However, its
16 co-localization with Nedd4L was not detected (Appendix Fig S2A), because exogenous
17 expression of Nedd4L-green fluorescent protein (GFP) stimulated ENaC internalization,
18 resulting in the disappearance of α ENaC from the cell surface. Cell-surface α ENaC was
19 observed in cells lacking Nedd4L-GFP expression (non-transfected cells). When a
20 catalytically inactive Nedd4L mutant, C922A, was expressed, it co-localized with cell-
21 surface α ENaC and endogenous FCHO2 (Fig 2B). The mutant also formed FCHO2-
22 negative spots. In wild-type HeLa cells, Nedd4L accumulated at clathrin-coated
23 structures where FCHO2 localized (Fig 2C). Additionally, Nedd4L formed clathrin-

1 negative spots, suggesting that they may be involved in clathrin-independent
2 endocytosis.

3 Using total internal reflection fluorescence (TIRF) microscopy, we investigated
4 whether Nedd4L is recruited to CCPs in wild-type HeLa cells. Similar to FCHO2
5 described previously (Henne *et al*, 2010; Lehmann *et al*, 2019; Zaccai *et al*, 2022),
6 Nedd4L showed dynamic co-localization with clathrin during pit formation (Fig 3).
7 When both fluorescent protein-tagged FCHO2 and Nedd4L were expressed, the
8 accumulation of Nedd4L at FCHO2-positive spots was not clearly observed (Appendix
9 Fig S2B). The reason behind this remains unknown, but it has been shown that clathrin
10 coat formation, measured in time-lapse images of cells expressing fluorescent proteins,
11 is affected by several factors, such as overexpression level, choice of the proteins, and
12 choice of the fluorescent tag (Aguet *et al*, 2013). These factors may contribute to the
13 failure to detect the accumulation of Nedd4L at FCHO2-positive spots.

14 While Nedd4L shows a punctate staining pattern at the cell surface (see Figs
15 2C, 3B and 3C), it exhibited diffuse distribution throughout the cytoplasm (Fig 4A and
16 B). In COS7 cells, co-expression of the FCHO2 BAR domain [amino acid (aa) 1-302]
17 recruited Nedd4L to membrane tubules (Fig 4A). The Nedd4L C2 domain (Myc-
18 Nedd4L C2, aa 1-160) was also concentrated to membrane tubules, whereas C2 domain-
19 deleted Nedd4L (Myc-Nedd4L ΔC2) was not. In contrast to FCHO2, the FBP17 BAR
20 domain did not recruit Nedd4L to membrane tubules. Additionally, the BAR domain
21 protein amphiphysin1 did not recruit Nedd4L to membrane tubules. Thus, Nedd4L is
22 selectively recruited through the C2 domain to membrane tubules generated by the
23 FCHO2 BAR domain. Similar results were obtained in HEK293 cells (Fig 4B). In these

1 cells, membrane tubules generated by amphiphysin1 were hardly detected. It showed a
2 punctate staining pattern and did not co-localized with Nedd4L.

3 We also investigated whether the FCHO2 BAR domain not only recruits but
4 also activates Nedd4L in cells. For this purpose, we performed an *in vivo* ubiquitination
5 assay using HEK293 cells, which formed membrane tubules upon FCHO2 expression
6 more efficiently than did COS7 cells: $91 \pm 2\%$ of HEK293 cells vs. $32 \pm 2\%$ of COS7
7 cells [the mean \pm standard error of the mean (S.E.M.) of four independent experiments].
8 As the catalytic activity of E3 Ub ligases is typically reflected in their
9 autoubiquitination (Wiesner *et al*, 2007), we determined activity by measuring the
10 ubiquitination level of Nedd4L itself. Expression of the FCHO2 BAR domain in cells
11 remarkably enhanced Nedd4L autoubiquitination, whereas FBP17 or amphiphysin1 did
12 not (Fig 5A). Tubulation-deficient FCHO2 mutants (K146E+R152E and L136E)
13 (Henne *et al*, 2010) did not enhance Nedd4L activity (Fig 5A–C and Fig EV3). A
14 catalytically inactive Nedd4L mutant, C922A, which was recruited to FCHO2-generated
15 membrane tubules, showed little enhancement of ubiquitination upon FCHO2
16 expression (Fig 5D and E), indicating that Nedd4L ubiquitination is self-induced. Using
17 α ENaC as a substrate, we further confirmed that Nedd4L is activated upon FCHO2
18 expression in cells (Fig 5F).

19

20 **Preference of Nedd4L for FCHO2-generated membrane curvature**

21 The aforementioned results prompted us to investigate whether FCHO2 and Nedd4L
22 interact through membrane tubules rather than through stereotyped protein–protein
23 interactions. Membrane tubules generated by BAR domains in cells have specific

1 diameters (curvatures) (Henne *et al*, 2007; Peter *et al*, 2004; Takano *et al*, 2008; Takei *et*
2 *al*, 1999; Yin *et al*, 2009). Nedd4L may preferentially bind to the specific degree of
3 membrane curvature generated by FCHO2. To investigate this possibility, we first
4 examined the biochemical properties of Nedd4L. Using a co-sedimentation assay with
5 liposomes containing various percentages of PS, we found that the C2 domain of
6 Nedd4L is a Ca^{2+} -dependent PS-binding domain (Fig 6A and B). Submicromolar Ca^{2+}
7 concentrations, which are comparable to intracellular levels in unstimulated cells, were
8 sufficient for the Nedd4L C2 domain to bind to PS-containing liposomes. The C2
9 domain alone and full-length Nedd4L showed different Ca^{2+} requirements. The higher
10 Ca^{2+} requirement of full-length Nedd4L may be due to the intramolecular interaction
11 between the C2 and HECT domains. Increasing PS percentages in synthetic liposomes
12 enhanced the liposome binding of the Nedd4L C2 domain, and PS requirements varied
13 depending on Ca^{2+} concentration.

14 We next examined whether Nedd4L preferentially binds to a specific degree of
15 membrane curvature. For this purpose, liposomes of different sizes (curvatures) were
16 prepared by stepwise extrusion through filter membranes with different pore sizes (0.8,
17 0.4, 0.2, 0.1, 0.05, and 0.03 μm) and sonication. Sonication or extrusion through a 0.03
18 μm pore-size filter was used to prepare the smallest liposomes. Transmission electron
19 microscopy revealed that the actual liposome size was similar to the pore size for 0.2,
20 0.1, 0.05, and 0.03 μm pore-size liposomes, whereas it was significantly smaller for 0.8
21 and 0.4 μm pore-size liposomes (Fig 7A). Nedd4L showed the strongest binding to 0.05
22 μm pore-size liposomes (Fig 7B).

23 Synaptotagmin I (SytI) tandem C2 domains can both generate and sense

membrane curvature *in vitro* by penetrating their hydrophobic residues into the lipid bilayer (Martens *et al*, 2007). As a sensor, the binding affinity is considered to be highest for membranes that have a degree of curvature consistent with that generated by SytI itself. We investigated whether, in addition to sensing membrane curvature, the Nedd4L C2 domain can also generate membrane curvature *in vitro* and, if so, what diameter of membrane tubules is generated. As expected, transmission electron microscopy revealed that the C2 domain deformed liposomes into extensive tubulation (Fig 7C). It should be noted that Nedd4L does not generate membrane tubules in cells (see Fig 4A and B). The tubule diameter generated by Nedd4L *in vitro* was mainly 40–80 nm, which is consistent not only with the diameter of 0.05 μm pore-size liposomes, to which Nedd4L preferentially binds, but also with the diameter of membrane tubules generated by FCHO2 (Fig 7D). These results suggest that Nedd4L shows the highest binding affinity for the degree of membrane curvature generated by FCHO2. It is therefore likely that FCHO2-induced recruitment and activation of Nedd4L are mediated by the degree of membrane curvature.

16

17 **Roles of conserved hydrophobic residues in the Nedd4L C2 domain**

18 We compared the C2 domain sequence of Nedd4L to those of other Nedd4 family
19 members, SytI, and PKCγ (Fig 8A). SytI C2 domains possess hydrophobic residues
20 (M173, F234, V304, and I367) for penetration into the lipid bilayer to generate and
21 sense membrane curvature (Martens *et al*, 2007). The Nedd4L C2 domain also has three
22 hydrophobic residues (I37, F38, and L99), which are conserved among Nedd4 family
23 members except for WWP2. We mutated these residues to alanine to produce six

1 mutants, I37A, F38A, L99A, I37A+F38A, I37A+L99A, and I37A+F38A+L99A (triple-
2 A). Any single mutation did not inhibit Nedd4L recruitment to FCHO2-generated
3 membrane tubules (Fig 8B). However, double and triple mutations severely impaired
4 this recruitment. Furthermore, the I37A+F38A and triple-A mutants showed little
5 liposome binding and lost curvature generation (Fig 8C and D). Thus, these
6 hydrophobic residues (I37, F38, and L99) are critical for both membrane binding and
7 curvature sensing and generation. These residues are likely inserted into the lipid
8 bilayer, thereby strengthening the C2 domain interaction with membranes and enabling
9 the sensing and generation of membrane curvature. It has been shown that I37 and F38
10 are directly involved in Ca^{2+} binding (Escobedo *et al*, 2014). The residues may be
11 inserted into the lipid bilayer while binding Ca^{2+} .

12 In the C2 domain of Smurf2, another Nedd4 family member, conserved
13 hydrophobic residues (F29 and F30) are responsible for interactions with the HECT
14 domain (Fig 8A) (Wiesner *et al*, 2007). Mutation at these residues impairs the
15 interaction between the C2 and HECT domains, resulting in enhanced Smurf2
16 autoubiquitination by relieving autoinhibition. Consistent with these previous findings,
17 we found that the Nedd4L I37A+F38A mutant, which was not recruited to FCHO2-
18 generated membrane tubules, enhanced autoubiquitination, irrespective of FCHO2
19 expression (Fig 5D and E). These results suggest that I37 and F38 are critical for
20 interactions with the HECT domain as well as for membrane binding and curvature
21 sensing. Interestingly, the Nedd4L I37A+F38A mutant, as well as the C922A mutant,
22 showed little αENaC ubiquitination (Fig EV4), indicating that membrane binding of
23 Nedd4L is critical for ENaC ubiquitination.

1

2 ***In vitro* activation of Nedd4L by FCHO2-generated membrane curvature**

3 To examine the properties of Nedd4L catalytic activity, we carried out an *in vitro*
4 ubiquitination assay using an α ENaC peptide as a substrate. The α ENaC peptide
5 possesses a conserved PY motif for interaction with the Nedd4L WW domain, and it is
6 fused with monomeric streptavidin (mSA) (Lim *et al*, 2013) to bind to liposomes
7 containing biotinylated phospholipids (biotinylated liposomes) (Sakamoto *et al*, 2017)
8 (Fig 9A and B). We found that Ca^{2+} and PS were required for Nedd4L catalytic activity
9 (Fig 9C and D), and that 0.05 μm pore-size liposomes were most effective in
10 stimulating Ca^{2+} - and PS-dependent Nedd4L activity (Fig 9E). Thus, the properties of
11 Nedd4L catalytic activity are similar to those of its liposome binding. Furthermore, we
12 found that Nedd4L did not ubiquitinate PY motif-mutated (Y644A in α ENaC) mSA-
13 α ENaC (Appendix Fig S3). These findings are consistent with defects in ENaC
14 ubiquitination observed in Liddle syndrome.

15 We next examined whether membrane localization of mSA- α ENaC affects the
16 membrane binding and catalytic activity of Nedd4L. Nedd4L bound only slightly to
17 mSA- α ENaC on PS-free (0% PS) liposomes, but the liposome binding was
18 synergistically increased by elevating the PS percentage in liposomes (Fig 9F). By
19 contrast, when free biotin competitively inhibited the binding of mSA- α ENaC to
20 biotinylated liposomes, the PS-dependent liposome binding of Nedd4L was
21 significantly reduced, resulting in remarkable inhibition of mSA- α ENaC ubiquitination
22 (Fig 9D and F). Thus, membrane localization of the PY motif is critical for membrane
23 binding and activation of Nedd4L. It is, therefore, likely that the PY motifs on

1 membranes, such as ENaC, play a role in enhancing Nedd4L catalytic activity by
2 potentiating membrane binding through interactions with the WW domain.

3 We then reconstituted *in vitro* FCHO2-induced recruitment and activation of
4 Nedd4L. When liposomes (20% PS) were used, the FCHO2 BAR domain enhanced the
5 liposome binding of Nedd4L (Fig 10A) and mSA- α ENaC ubiquitination (Fig 10B). This
6 enhancement was lost when the strength of interaction of Nedd4L with liposomes was
7 increased by elevating the PS percentage in liposomes (~50% PS) (Fig 10C and Fig
8 EV5). In contrast to FCHO2, neither amphiphysin1 nor FBP17 enhanced Nedd4L
9 activity (Fig 10D and Fig EV6A). Similarly, tubulation-deficient FCHO2 mutant
10 (L136E) did not enhance Nedd4L activity (Fig 10E and Fig EV6A). These results are in
11 good agreement with those obtained from *in vivo* experiments on FCHO2-induced
12 recruitment and activation of Nedd4L. Electron microscopic analysis revealed that
13 mSA- α ENaC-associated liposomes were deformed by membrane-sculpting proteins into
14 tubules with diameters similar to those of mSA- α ENaC-free liposomes (Fig EV6B and
15 see also Fig 7D). The diameter of membrane tubules generated by FCHO2 is consistent
16 with that of 0.05 μ m pore-size liposomes which are most effective in stimulating
17 Nedd4L activity.

18 To confirm whether FCHO2-induced recruitment and activation of Nedd4L are
19 mediated by liposomes (i.e., membrane curvature) rather than by protein–protein
20 interactions, we conducted two sets of experiments. Initially, we employed synthetic
21 liposomes where 20% PS was substituted with 5% PI(4,5)P₂. The FCHO2 BAR domain
22 bound to PI(4,5)P₂ as well as PS with high affinity, whereas the Nedd4L C2 domain did
23 not (Fig 11A and B). The FCHO2 BAR domain is known to induce the tubulation of

1 liposomes [5% PI(4,5)P₂] (Henne *et al*, 2010). If Nedd4L could interact through
2 protein–protein interactions with the FCHO2 BAR domain binding to liposomes [5%
3 PI(4,5)P₂], the BAR domain would facilitate the co-precipitation of Nedd4L in a co-
4 sedimentation assay, thereby stimulating mSA- α ENaC ubiquitination. However, the
5 FCHO2 BAR domain did not demonstrate such interactions (Fig 11C and D). Therefore,
6 it is unlikely that Nedd4L interacts with the FCHO2 BAR domain on liposomes through
7 protein–protein interactions. Secondly, we employed 0.05 μ m pore-size liposomes that
8 are most effective in stimulating Nedd4L activity. The diameter of 0.05 μ m pore-size
9 liposomes is consistent with that of membrane tubules generated by the FCHO2 BAR
10 domain. The BAR domain is, thus, expected not to induce the tubulation of 0.05 μ m
11 pore-size liposomes. The FCHO2 BAR domain showed similar binding activity toward
12 0.8 and 0.05 μ m pore-size liposomes (Fig 12A). When 0.8 μ m pore-size liposomes were
13 used, the FCHO2 BAR domain enhanced Nedd4L activity (Fig 12B). However, in the
14 case of 0.05 μ m pore-size liposomes, curvature-stimulated Nedd4L activity was not
15 potentiated by the addition of the FCHO2 BAR domain. If Nedd4L had interacted with
16 the BAR domain, we would have expected potentiation of Nedd4L activity. These
17 results strongly suggest that FCHO2-induced activation of Nedd4L is mediated by
18 membrane curvature and not by protein–protein interactions.

19

20 **Discussion**

21

22 Nedd4L represents the ancestral Ub ligase with strong similarity to yeast Rsp5 which
23 plays a key role in the trafficking, sorting, and degradation of a large number of proteins

1 (Yang & Kumar, 2010). Consistently, Nedd4L regulates a growing number of substrates,
2 including membrane receptors, transporters, and ion channels. Although Nedd4L exists
3 in a catalytically autoinhibited state due to an intramolecular interaction between the N-
4 terminal C2 and C-terminal HECT domains, little is known about its activation
5 mechanism. In this study, we clearly demonstrated that Nedd4L is activated by FCHO2
6 F-BAR domain-induced membrane curvature. It has been shown that the activity of
7 synptojanin-1, a phosphoinositide phosphatase, is modulated by membrane curvature
8 (Chang-Ileto *et al*, 2011). Taken together, it is conceivable that membrane curvature
9 serves as a signal for the activation of various enzymes involved in membrane
10 trafficking.

11

12 Unique Properties of the Nedd4L C2 Domain

13 Although both sytI and Nedd4L C2 domains are Ca^{2+} -dependent PS-binding domains
14 that can generate and sense membrane curvature, their properties show a number of
15 significant differences. An interesting difference exists in the degrees of membrane
16 curvatures generated by sytI and Nedd4L: the diameters of their membrane tubules are
17 about 15–20 nm and 40–80 nm, respectively (Hui *et al*, 2009; Martens *et al*, 2007). This
18 difference is not simply due to that between tandem and single C2 domains, because it
19 has been shown that the sytI C2B domain alone generates membrane tubules with a
20 similar diameter (Hui *et al*, 2009). SytI and Nedd4L C2 domains must therefore have
21 respective unique structures that determine the specific degrees of membrane curvatures
22 that they sense and generate.

23 Another important difference between sytI and Nedd4L C2 domains exists in

their Ca^{2+} requirements. SytI C2 domains require Ca^{2+} concentrations in the submillimolar range to generate membrane curvature (Hui *et al*, 2009). In contrast, submicromolar Ca^{2+} concentrations, which are comparable to intracellular levels in unstimulated cells, are sufficient for the Nedd4L C2 domain to sense membrane curvature. This is consistent with the observation that Nedd4L is recruited and activated in serum-starved cells. The different Ca^{2+} requirements between sytI and Nedd4L C2 domains are reflected in their functions. SytI C2 domains induce membrane curvature in response to an increase in intracellular Ca^{2+} concentration, which is essential for Ca^{2+} -triggered membrane fusion (Hui *et al*, 2009; Martens *et al*, 2007). Thus, sytI C2 domains serve as a Ca^{2+} sensor and a curvature generator. In contrast, the Nedd4L C2 domain recognizes a specific degree of curvature without an increase in intracellular Ca^{2+} concentration. Therefore, the Nedd4L C2 domain serves as a curvature sensor to regulate the localization and activity of the E3 Ub ligase.

A striking feature that distinguishes the Nedd4L C2 domain from other C2 domain proteins (except for at least a subset of Nedd4 family members) is that the Nedd4L C2 domain interacts not only with membranes but also with the intramolecular catalytic domain for its autoinhibition. Mutational experiments have revealed that I37 and F38 residues in the C2 domain are critical for interactions with both membranes and the HECT domain, suggesting that these two interactions are competitive. This idea is supported by the observation that the Ca^{2+} EC₅₀ value of full-length Nedd4L is much higher than that of the C2 domain. The HECT domain in full-length Nedd4L may competitively inhibit the interaction of the C2 domain with membranes. It is likely that membranes displace the HECT domain from the C2 domain when the strength of the C2

1 domain interaction with membranes is increased by the preferred membrane curvature.
2 This displacement relieves the autoinhibition, resulting in Nedd4L activation. Thus, the
3 membrane binding of Nedd4L is coupled with its activation.

4

5 **Stimulatory and inhibitory effects of the FCHO2 BAR domain on the liposome
6 binding and catalytic activity of Nedd4L**

7 The FCHO2 BAR domain enhances both the liposome binding and catalytic activity of
8 Nedd4L when the interaction strength of Nedd4L with liposomes is weak (20% PS) (Fig
9 10A and B). Conversely, the BAR domain inhibits the binding and activity of Nedd4L
10 when the interaction of Nedd4L with liposomes is increased by elevating the PS
11 percentage in liposomes (~50% PS) (Fig 10C and Fig EV5). Thus, the FCHO2 BAR
12 domain exerts both stimulatory and inhibitory effects on Nedd4L, depending on the PS
13 percentage in liposomes. However, given that 20% PS is comparable to the
14 concentration in the inner leaflet of the plasma membrane, it is plausible that FCHO2
15 exhibits only a stimulatory effect on Nedd4L in cells. The mechanism underlying the
16 stimulatory and inhibitory effects *in vitro* is as follows: when using liposomes (20%
17 PS), Nedd4L hardly binds to liposomes through PS (Fig. 9F and 10A). The addition of
18 the FCHO2 BAR domain enhances the strength of Nedd4L's interaction with PS by
19 inducing membrane curvature. Consequently, Nedd4L gains a new binding to liposomes
20 through PS, which augments its catalytic activity. In contrast, when using liposomes
21 (~50% PS), Nedd4L binds to liposome through PS. The addition of the FCHO2 BAR
22 domain hinders the PS-mediated liposome binding of Nedd4L, because FCHO2 and
23 Nedd4L are PS-binding proteins and compete for PS binding in liposomes.
24 Consequently, the BAR domain inhibits the catalytic activity of Nedd4L. This is
25 consistent with the results obtained with 0.05 μm pore-size liposomes (Fig 12B). These
26 0.05 μm pore-size liposomes are comparable to liposomes with a higher PS percentage,

1 as the interaction of Nedd4L with liposomes through PS is increased by membrane
2 curvature. Therefore, when using 0.05 μ m pore-size liposomes, the FCHO2 BAR
3 domain inhibits the catalytic activity of Nedd4L.

4 Based on a model in which a subset of BAR domain proteins, such as FCHO2
5 and FBP17, drive liposome tubulation *in vitro* (Frost *et al*, 2008; Shimada *et al*, 2007),
6 the FCHO2 BAR domain is considered to polymerize on the liposome surface into
7 spiral dense coats by lateral and tip-to-tip interactions. When using liposomes (~50%
8 PS), it is conceivable that the FCHO2 BAR domain densely packs the liposomes,
9 leaving little free space for Nedd4L binding. Conversely, when using liposomes (20%
10 PS), it is likely that the liposomes are loosely packed, providing ample surface space for
11 Nedd4L binding.

12

13 **Model for ENaC Endocytosis**

14 Based on the present study, we propose a model for ENaC endocytosis through
15 ubiquitination (Fig 13). First, FCHO2 binds to the plasma membrane and generates a
16 specific degree of membrane curvature. FCHO2 interacts with clathrin adaptor proteins,
17 such as Eps15, and recruits the clathrin machinery for CCP formation (Uezu *et al*, 2011;
18 Henne *et al*, 2010). Eps15 has Ub-interacting motifs (Di Fiore *et al*, 2003). Nedd4L is
19 subsequently recruited to and activated by FCHO2-generated curved membrane at the
20 rim of nascent CCPs that ENaC enters. ENaC is then ubiquitinated and captured by
21 Eps15 which FCHO2 interacts with. Thus, ubiquitinated ENaC is spatially restricted to
22 CCPs and separated from unmodified ENaC. Overall, our findings suggest that in the
23 early stage of CME, a membrane deformation induced by FCHO2 can program, through
24 both the recruitment and activation of Nedd4L, the gathering of a subclass of cargo

1 molecules in CCPs.

2

1 **Methods**

2

3 **Construction**

4 Human α ENaC, β ENaC and γ ENaC cDNAs were kindly supplied by Dr. H. Kai
5 (Kumamoto University, Kumamoto, Japan) (Sugahara *et al*, 2009). FLAG- α ENaC was
6 constructed by replacing the sequence [amino acid (aa) 169–174, TLVAGS] in the
7 extracellular region with the FLAG sequence (DYKDDDK) as described previously
8 (Firsov *et al*, 1996). This introduction of the epitope tag was carried out by polymerase
9 chain reaction (PCR). FLAG- α ENaC, β ENaC, and γ ENaC were subcloned into pTRE-
10 Tight-Hygro, pCAGI-Puro (Miyahara *et al*, 2000), and pCAGI-Bst (Umeda *et al*, 2006),
11 respectively. pTRE-Tight-Hygro was constructed by inserting the hygromycin-
12 resistance gene into pTRE-Tight (Clontech). FLAG- α ENaC was also subcloned into
13 pCAGI-Hygro, which was constructed by replacing the puromycin-resistance gene of
14 pCAGI-Puro with the hygromycin-resistance gene. Human Nedd4L (NM_015277,
15 isoform 3) cDNA was obtained by reverse transcription (RT)-PCR and cloned in
16 pCMV-Myc (Miyahara *et al*, 2000). Nedd4L was also cloned in pCAGI-puro-EGFP and
17 pGEX-6P-hexahistidine (His6). pGEX-6P-His6 was constructed from pGEX-6P (GE
18 Healthcare) to express an N-terminal GST-tagged, C-terminal His6-tagged protein.
19 pCAGI-puro-EGFP was constructed by subcloning EGFP cDNA into pCAGI-puro to
20 express a C-terminal GFP-tagged protein. The Nedd4L C2 domain (C2, aa 1–160) and
21 C2 domain-deleted mutant (Δ C2, aa 150–955) were subcloned into pCMV-Myc and/or
22 pGEX-6P. Mouse FCHO2 (full length, aa 1–809; BAR domain, aa 1–302) and human
23 FBP17 (BAR domain, aa 1–300) were subcloned into pEGFP-C1 and/or pGEX-6P

1 (Uezu *et al*, 2011; Tsujita *et al*, 2006). FCHO2 (aa 1–327) were subcloned into pGEX-
2 6P. Human amphiphysin1 cDNA was obtained by RT-PCR and cloned in pEGFP-N3.
3 Amphiphysin1 (BAR domain, aa 1–377) was then subcloned into pGEX-6P. mTagRFP-
4 T-Clathrin-15 was a gift from Michael Davidson (Addgene plasmid # 58005 ;
5 <http://n2t.net/addgene:58005> ; RRID:Addgene_58005) (Shaner *et al*, 2008). Human
6 hemagglutinin (HA)-tagged Ub cDNA in pCGN was kindly donated by Dr. M. Nakao
7 (Kumamoto University, Kumamoto, Japan). Ub cDNA was subcloned into pET3a.
8 Human UbcH7 cDNA was obtained by RT-PCR and cloned in pGEX-6P. pET21d-
9 Ube1 was a gift from Cynthia Wolberger (Addgene plasmid # 34965 ;
10 <http://n2t.net/addgene:34965> ; RRID:Addgene_34965) (Berndsen & Wolberger, 2011).
11 pRSET-mSA was a gift from Sheldon Park (Addgene plasmid # 39860 ;
12 <http://n2t.net/addgene:39860> ; RRID:Addgene_39860) (Lim *et al*, 2013). mSA- α ENaC
13 constructed in pRSET-mSA to express a fusion protein of the N-terminal (aa 7–40) and
14 C-terminal (aa 625–659) intracellular regions of α ENaC (see Fig. 9A). Mutagenesis was
15 performed by PCR using mutated primers and a site-directed mutagenesis kit
16 (Stratagene).
17

18 Protein expression and purification

19 Expression and purification of GST-tagged proteins were performed using standard
20 protocols. His6-tagged proteins were purified with Talon metal affinity resin (Clontech)
21 using the manufacturer's protocol. The GST tag was cleaved off by PreScission
22 protease (GE Healthcare). The GST tag of BAR domains did not inhibit liposome
23 binding or tubulation, whereas the GST tag of Nedd4L inhibited these functions. As

1 FCHO2 (BAR domain, aa 1–302) was easily aggregated by the removal of the GST tag,
2 FCHO2 (aa 1–327) was used instead as a GST-cleaved form of the FCHO2 BAR
3 domain. Full-length Nedd4L (N-terminal GST-tagged, C-terminal His6-tagged) was
4 purified by glutathione–Sepharose (GE Healthcare) column chromatography. The GST
5 tag was cleaved off and the Nedd4L sample was then subjected to Talon metal affinity
6 column chromatography. After the eluate was passed through glutathione–Sepharose
7 beads, the sample was dialyzed against buffer A (20 mM Tris-HCl at pH 7.5, 100 mM
8 KCl, 0.5 mM EDTA, 1 mM DTT, and 20 % sucrose). The Nedd4L sample was stored at
9 –80°C until use. Ub was expressed in *E. coli* strain BL21 (DE3) pJY2 and purified as
10 previously described (Pickart & Raasi, 2005). His6-tagged mSA- α ENaC was expressed
11 in *E. coli* strain BL21 (DE3) pLysS and purified as previously described (Lim *et al*,
12 2013) with slight modifications. Briefly, the inclusion body was isolated and solubilized
13 in buffer B (50 mM Tris-HCl at pH 8.0 and 6 M guanidine hydrochloride). The sample
14 was then subjected to Talon metal affinity column chromatography. The eluate was
15 added drop by drop to ice-cold refolding buffer (50 mM Tris-HCl at pH 8.0, 150 mM
16 NaCl, 0.15 mg/ml D-biotin, 0.2 mg/ml oxidized glutathione, and 1 mg/ml reduced
17 glutathione) under rapid stirring. The sample was then concentrated using a Centriprep
18 centrifugal filter unit (Millipore) and centrifuged to remove aggregates. The supernatant
19 was dialyzed against buffer C (20 mM Tris-HCl at pH 8.0). The mSA- α ENaC sample
20 was further purified by Mono Q anion exchange column chromatography as follows.
21 The sample was applied to a Mono Q 5/50 GL column (GE Healthcare) equilibrated
22 with buffer C. Elution was performed with a 50 ml linear gradient of NaCl (0–200 mM)
23 in buffer C. Fractions of 1 ml each were collected. The active fractions (fraction 18–22)

1 were collected and dialyzed against buffer D (10 mM Tris-HCl at pH 7.5, 100 mM KCl,
2 and 0.5 mM EDTA). The mSA- α ENaC sample was stored at -80°C until use.

3

4 **Antibodies**

5 Rabbit anti-Nedd4L antibody was raised against GST-Nedd4L C2 (aa 1–160). Rabbit
6 anti-FCHO2 antibody was obtained as previously described (Uezu *et al*, 2011). The
7 following antibodies were purchased from commercial sources: mouse anti-Myc (9E10)
8 (American Type Culture Collection); mouse anti-FLAG (M2) and mouse anti- α -tubulin
9 (clone DM1A) (Sigma-Aldrich); mouse anti-clathrin heavy chain (BD Biosciences);
10 rabbit anti-GFP (MBL Co.); rabbit anti- α ENaC (Calbiochem); rabbit anti- β ENaC
11 (Proteintech); rabbit anti- γ ENaC (Abcam); mouse anti-transferrin receptor H68.4 (Santa
12 Cruz); mouse anti-Ub antibody P4D1 (Santa Cruz); and secondary antibodies
13 conjugated with Alexa Fluor 488, 594, and 647 (Invitrogen).

14

15 **Cell culture and transfection**

16 HeLa, HEK293, and COS7 cells were cultured in Dulbecco's modified Eagle medium
17 (DMEM) supplemented with 10% fetal calf serum. HEK293 cells were grown on poly-
18 L-lysine-coated dishes. Transfection was performed by using Lipofectamine 2000
19 (Invitrogen) according to the manufacturer's protocol.

20

21 **Generation of stable HeLa cells expressing all three ENaC subunits**

22 HeLa cells were transfected with the pTet-On Advanced vector (Clontech) to develop
23 stable Tet-On cell lines for a doxycycline (Dox)-inducible expression system according

1 to the manufacturer's protocol. Tet-On cells were selected in 0.5 mg/ml G418. Cloned
2 Tet-On cells were then transfected with pCAGI-Bst- γ ENaC and selected in 4 μ g/ml
3 blasticidin (in the presence of G418). Blasticidin-resistant cells were transfected with
4 pCAGI-Puro- β ENaC and selected in 1 μ g/ml puromycin (in the presence of G418 and
5 blasticidin). Puromycin-resistant cells were finally transfected with pTRE-Tight-Hygro-
6 FLAG- α ENaC and cultured in 0.2 mg/ml hygromycin (in the presence of G418,
7 blasticidin, and puromycin). After selection, cells were cloned and maintained in 0.5
8 mg/ml G418, 0.2 mg/ml hygromycin, 1 μ g/ml puromycin, and 2.5 μ g/ml blasticidin.
9 FLAG-tagged α ENaC expression was induced by treating cells with 1 μ g/ml Dox in the
10 presence of 40 μ M amiloride overnight. Amiloride was added to prevent cellular Na⁺
11 overload.

12

13 Immunofluorescence microscopy

14 Cells were fixed with 3.7% formaldehyde in phosphate-buffered saline (PBS) at room
15 temperature for 15 min, and then permeabilized with 0.2% Triton X-100 in PBS for 10
16 min. After blocking with 1% bovine serum albumin (BSA) in PBS, cells were
17 sequentially incubated with primary antibodies and fluorescence-conjugated secondary
18 antibodies at room temperature for 1 h, respectively. Cells were then analyzed with
19 either a fluorescence microscope (BX51; Olympus) or a confocal microscopy system
20 (BX50, Fluoview FV300, and Fluoview FV1200; Olympus). A 60 \times oil immersion
21 objective (NA = 1.40, Olympus) was used. All comparable images were acquired under
22 identical parameters. To visualize cell-surface FLAG- α ENaC in $\alpha\beta\gamma$ ENaC-HeLa cells,
23 cells were incubated with 5 μ g/ml anti-FLAG M2 antibody at 4°C for 1 h to prevent

1 internalization. Cells were then fixed, permeabilized, and stained with a secondary
2 antibody. Cells were also sequentially incubated with primary (anti-FCHO2) and
3 secondary antibodies. To quantify co-localization, the Pearson's correlation coefficient
4 was calculated from three cells using the Fiji (ImageJ) Coloc2 plug-in.

5

6 RNA interference

7 Stealth™ double-stranded RNAs were purchased from Invitrogen. siRNA sequences of
8 human FCHO2, Nedd4L, and FBP17 were 5'-CCA CAG AUC UUA GAG UGG AUU
9 AUA A-3' (corresponding to nucleotides 2048–2072 relative to the start codon), 5'-GAA
10 GAG UUG CUG GUC UGG CCG UAU U-3' (corresponding to nucleotides 1778–1802
11 relative to the start codon), and 5'-CCC ACU UCA UAU GUC GAA GUC UGU U-
12 3'for human FBP17 (corresponding to nucleotides 1804–1828 relative to the start
13 codon), respectively. A double-stranded RNA targeting luciferase (GL-2, 5'-CGU ACG
14 CGG AAU ACU UCG AAA UGU C-3') was used as a control. HeLa cells were
15 transfected with 20 nM siRNA using Lipofectamine 2000 according to the
16 manufacturer's protocol. After 24 h, a second transfection was performed, and cells
17 were cultured for 3 days and subjected to various experiments. For rescue experiments,
18 cells were transfected with the intended plasmid at 36 h after the second transfection.
19 After 18 h, cells were fixed and analyzed.

20

21 Quantitative real-time PCR analysis

22 Total RNA was isolated using ISOGEN (Nippon Gene, 319-90211), and cDNA was
23 synthesized using ReverTra Ace qPCR RT Master Mix with gDNA Remover (Toyobo,
24 FSQ-301), following manufacturer's instruction. Real time PCR was carried out using

1 Thunderbird Next SYBR (Toyobo, QPX-201) on StepOnePlus Real-Time PCR Systems
2 (Applied Biosystems). The sequences of qPCR primers are 5'-TCT CCC ATC GCT
3 TCA ACG AG-3' and 5'-GTT GCA CCC AGC TTG AGA GA-3' for human FBP17; 5'-
4 GTC TCC TCT GAC TTC AAC AGC G-3' and 5'-ACC ACC CTG TTG CTG TAG
5 CCA A-3' for human GAPDH. The expression of target genes was normalized to
6 GAPDH mRNA levels.

7

8 **Endocytosis assay**

9 $\alpha\beta\gamma$ ENaC-HeLa cells at approximately 90% confluence in a 10-cm dish were starved
10 with serum-free medium (DMEM containing 1% BSA, 1 μ g/ml Dox, and 40 μ M
11 amiloride) at 37°C for 4 h. For ENaC endocytosis, cells were then incubated with 5
12 μ g/ml anti-FLAG M2 in 2 ml of DMEM containing 1% BSA at 4°C for 1 h to prevent
13 internalization. After three washes with ice-cold PBS containing 1 mM MgCl₂ and 0.1
14 mM CaCl₂ (PBS-CM), endocytosis was allowed by incubating cells in prewarmed
15 DMEM containing 1% BSA at 37°C for the indicated periods of time. Endocytosis was
16 stopped by placing cells on ice and washing them with ice-cold PBS-CM. Antibody
17 bound to the cell surface but not internalized was removed by acid stripping with 0.2 M
18 acetic acid and 0.5 M NaCl solution (pH 2.5). After washing with ice-cold PBS-CM,
19 internalized ENaC was detected by immunoblotting (IB) or immunofluorescence
20 microscopy. For IB, cells were scraped in 1 ml of lysis buffer A (50 mM Tris-HCl at pH
21 8.0, 150 mM NaCl, 5 mM EDTA, 1% Triton X-100, 1 mM PMSF, 20 μ g/ml leupeptin,
22 and 1 μ g/ml pepstatin A). Cells were solubilized at 4°C for 1 h on a rotating wheel, and
23 centrifuged at 20,000 \times g at 4°C for 15 min. Protein G-Sepharose beads (GE
24 Healthcare) were added to the supernatant and incubated at 4°C for 3 h. The beads were
25 then thoroughly washed with lysis buffer A and boiled in sodium dodecyl sulfate (SDS)
26 sample buffer. The sample was subjected to SDS-polyacrylamide gel electrophoresis

1 (PAGE), followed by IB with anti-ENaC subunit antibodies. Internalization was
2 expressed as a percentage of the initial amount of cell-surface ENaC subunit determined
3 by incubating cells with anti-FLAG antibody at 4°C for 1 h and lysing them without
4 incubation at 37°C or acid stripping. For immunofluorescence microscopy, cells were
5 transfected with control or FCHO2 siRNA and then with GFP-siRNA-resistant (sr)
6 FCHO2 mutant. After cells were labeled with anti-FLAG antibody on 4°C, they were
7 incubated at 37°C for 10 min to allow ENaC endocytosis. After acid stripping, cells
8 were fixed with 3.7% formaldehyde and permeabilized with 0.2% Triton X-100. The
9 antibody-labeled, internalized α ENaC was visualized with a fluorescence-conjugated
10 secondary antibody. The percentage of cells with internalized α ENaC among cells
11 expressing GFP-sr-FCHO2 was determined using MetaMorph imaging System
12 software. All images were acquired under identical parameters. For TfR endocytosis, a
13 cell surface biotinylation assay was carried out as previously described (Roberts *et al*,
14 2001). Briefly, the cell surface was labeled with Sulfo-NHS-SS-Biotin (Thermo Fisher
15 Scientific) at 4°C. After cells were incubated with ice-cold quenching buffer (50 mM
16 NH₄Cl in PBS-CM) at 4°C, they were incubated with serum free medium for 10 min at
17 37°C. Biotin was removed from the cell surface by incubation with ice-cold MesNa
18 buffer (50 mM MesNa, 100 mM NaCl, and 100 mM Tris-HCl, pH 8.8). Cells were then
19 incubated with iodoacetamide at 4°C. Cell lysates were then incubated with
20 NeutrAvidin beads (Thermo Fisher Scientific). The beads were boiled in SDS sample
21 buffer. Proteins were analyzed by IB with TfR antibody.

22

23 **ENaC expression and ubiquitination at the cell surface**

24 $\alpha\beta\gamma$ ENaC-HeLa cells at approximately 90% confluence in a 10-cm dish were starved
25 with serum-free medium (DMEM containing 1% BSA, 1 μ g/ml Dox, and 40 μ M
26 amiloride) at 37°C for 4 h, washed three times with ice-cold PBS, and incubated at 4°C

1 for 45 min with 2 ml of 1 mg/ml EZ-link Sulfo-NHS-SS-Biotin in PBS with gentle
2 shaking. Subsequently, cells were extensively washed with ice-cold Tris-buffered saline,
3 and then scraped into 1 ml of lysis buffer B (50 mM Tris-HCl at pH 7.5, 150 mM NaCl,
4 5 mM EDTA, 1% Triton X-100, 10 mM N-ethylmaleimide, 1 mM PMSF, 10 µg/ml
5 leupeptin, and 1 µg/ml pepstatin A) containing 40 µM MG132. Cells were solubilized at
6 4°C for 1 h on a rotating wheel, and centrifuged at 20,000 × g at 4°C for 15 min. The
7 supernatant (4 mg of protein) was incubated at 4°C for 3 h with 10 µg of anti-FLAG M2
8 antibody. Protein G-Sepharose beads (50 µl of 50% slurry) were then added to the
9 sample, which was incubated at 4°C for 3 h. After beads were thoroughly washed with
10 lysis buffer B containing 40 µM MG132, FLAG-tagged proteins were eluted from the
11 beads with 200 µg/ml FLAG peptide (Sigma-Aldrich) in 0.5 ml of lysis buffer B. After
12 centrifugation, the supernatant was incubated with 25 µl of NeutrAvidin beads at 4°C
13 overnight. After the beads were thoroughly washed with lysis buffer B, bound proteins
14 were eluted by incubating the beads at 4°C for 1 h with 150 µl of lysis buffer B
15 containing 200 mM DTT. After centrifugation, 5 × SDS sample buffer was added to the
16 supernatant, which was then analyzed by IB with anti-FLAG and anti-Ub antibodies.
17 The chemiluminescence intensity was quantified by scanning using ImageJ software
18 (NIH).

19

20 **TIRF Microscopy**

21 For live observation with TIRF microscopy, HeLa cells were grown on a glass-
22 bottomed dish as described previously (Shimada *et al*, 2007). Cells were observed at
23 10–12 h after transfection as described previously (Henne *et al*, 2010). Images were
24 acquired for 5 min at 1 s intervals with a TIRF microscopy system (Olympus), a 100 ×

1 oil immersion objective NA = 1.45 (Olympus) and MetaMorph Imaging System
2 Software. All comparable images were acquired under identical parameters.

3

4 **Liposome preparation**

5 Phospholipids were purchased from commercial sources: phosphatidylcholine (PC, 1,2-
6 dioleoyl-*sn*-glycero-3-phosphocholine), phosphatidylethanolamine (PE, 1,2-dioleoyl-*sn*-
7 glycero-3-phosphoethanolamine), PS (1,2-dioleoyl-*sn*-glycero-3-phospho-L-serine),
8 rhodamine-PE [18:1 L- α -PE-N-(lissamine rhodamine B sulfonyl)], PEG2000-biotin-PE
9 (1,2-distearoyl-*sn*-glycero-3-phosphoethanolamine-N-[biotinyl (polyethyleneglycol)-
10 2000]), porcine brain PS, brain PI(4,5)P₂, and porcine brain total lipid extract were
11 obtained from Avanti Polar Lipids; cholesterol and Folch lipids [bovine brain lipids
12 (Folch Fraction 1)] were obtained from Sigma-Aldrich; X-biotin-PE [N-((6-
13 biotinoyl)amino)hexanoyl]-1,2-dihexadecanoylsn-glycero-3-phosphoethanolamine]
14 was obtained from Thermo Fisher Scientific; and fluorescein-PE [N-(fluorescein-5-
15 thiocarbamoyl)-1,2-dihexadecanoyl-sn-glycero-3-phosphoethanolamine] was obtained
16 from AAT Bioquest Inc.

17 Liposomes were prepared using brain lipids (Folch lipids, ~50% PS of total
18 lipids), brain lipids (20% PS of total lipids, a mixture of 89.5% porcine brain total lipid
19 extract and 10.5% porcine brain PS), or a synthetic lipid mixture [70% PC, 20% PE,
20 10% cholesterol (w/w), and varying percentages of PS or PI(4,5)P₂ (with a
21 corresponding reduction in PC)]. Lipid concentrations were monitored by including 1%
22 rhodamine-PE (w/w). To prepare mSA- α ENaC-associated liposomes, 2% PEG2000-
23 biotin-PE (w/w) was included. Lipids were dried under nitrogen gas, desiccated for 2 h,
24 and resuspended at 1 mg/ml in lipid buffer (50 mM HEPES-NaOH at pH 7.2, 100 mM

1 KCl, 2 mM MgCl₂, and 5 mM EGTA), followed by hydration at 37°C for 1 h. To make
2 liposomes of different sizes, they were subjected to five freeze–thaw cycles and
3 centrifuged at 100,000 × g for 15 min. Precipitated liposomes were then resuspended in
4 the same buffer to make a final concentration of 1 mg/ml. They were subjected to
5 extrusion through polycarbonate filter membranes (Avanti Polar Lipids): liposomes
6 were sequentially passed 9 times through a 0.8-μm filter, 21 times through a 0.4-μm
7 filter, 21 times through a 0.2-μm filter, 21 times through a 0.1-μm filter, 21 times
8 through a 0.05-μm filter, and 21 times through a 0.03-μm filter. Instead of extrusion
9 through a 0.03-μm filter, liposomes with the smallest size were also prepared by
10 sonication three times for 5 s with a Branson Sonifier 25 at power level 1. Liposome
11 diameters were examined by transmission electron microscopy.

12

13 **Co-sedimentation assay**

14 A co-sedimentation assay was performed as described (Uezu *et al*, 2011) with slight
15 modifications. Briefly, 5–10 μg of protein was incubated at 25°C for 10 min with 0.5
16 mg/ml liposomes in 100 μl of lipid buffer containing various concentrations of CaCl₂
17 and centrifuged at 165,000 × g at 25°C for 15 min. Equal amounts of the supernatants
18 and pellets were subjected to SDS-PAGE, followed by Coomassie brilliant blue (CBB)
19 staining. Proteins were quantified by scanning using ImageJ (NIH). The assay with
20 liposomes of different sizes was performed using NeutrAvidin (Thermo Fisher
21 Scientific Inc) as described (Sakamoto *et al*, 2017). Briefly, brain-lipid (Folch-lipid)
22 liposomes (~50% PS) were supplemented with 1% X-biotin-PE and 1% rhodamine-PE,
23 subjected to extrusion through filter membranes, and then sonicated. Purified Nedd4L

1 protein (10 µg) was incubated with 0.2 mg/ml liposomes in 100 µl of lipid buffer
2 containing 2mM CaCl₂ (0.1 µM Ca²⁺). The sample was then incubated with 2 µg of
3 NeutrAvidin and ultracentrifuged. Both total and supernatant fluorescence were
4 measured. The proportion of precipitated liposomes of each size was ~100%.

5 The assay with mSA-αENaC-associated liposomes was performed as follows.

6 Liposomes were prepared from a synthetic lipid mixture [various percentages of PS or
7 5% PI(4,5)P₂] or brain lipids supplemented with 2% PEG2000-biotin-PE and 1%
8 rhodamine-PE. The liposomes (10 µg) were incubated with purified mSA-αENaC
9 protein (35 pmol) at 4°C for 10 min in 25 µl of lipid buffer. The sample was then
10 incubated at 25°C for 10 min with 0.07 µM (8 µg/ml) Nedd4L and/or 1.4 µM BAR
11 domains in 50 µl of ubiquitination buffer (50 mM HEPES-NaOH at pH 7.2, 100 mM
12 KCl, 2 mM MgCl₂, 5 mM EGTA, and 0.1 mM DTT) containing 4 mM CaCl₂ (0.7 µM
13 Ca²⁺). Subsequently, the sample was subjected to ultracentrifugation. Equal amounts of
14 the total samples and pellets were subjected to SDS-PAGE, followed by CBB staining
15 and IB. The chemiluminescence intensity was quantified by scanning using ImageJ
16 (NIH).

17 The assay with mSA-αENaC-associated liposomes (0.05 µm pore-size) was
18 done as follows. Liposomes were prepared from brain lipids (20% PS) supplemented
19 with 2% PEG2000-biotin-PE, 1% rhodamine-PE, and 0.5% fluorescein-PE (w/w) and
20 extruded through membrane filters. To precipitate liposomes, the sample (50 µl) was
21 first incubated with 1 µg of anti-fluorescein goat antibody (Novus Biologicals) at room
22 temperature for 1 h and then incubated with 0.5 µg of protein A/G/L (BioVision) at
23 room temperature for 1 h. Subsequently, the sample was centrifuged at 165,000 × g at

1 25°C for 15 min. Equal amounts of the supernatants and pellets were subjected to SDS-
2 PAGE, followed by CBB staining and IB. The percentage of precipitated liposomes was
3 ~100%.

4

5 **Calculation of free Ca²⁺ concentrations**

6 At 1.0, 2.0, 3.0, 3.5, 4.0, 4.5, and 4.9 mM CaCl₂ in lipid buffer, free Ca²⁺ concentrations
7 were calculated to be 0.04, 0.1, 0.3, 0.4, 0.7, 1.6, and 8.1 μM, respectively, as
8 determined by the Ca-Mg-ATP-EGTA Calculator v1.0 using constants from the NIST
9 database #46 v8. At 1.0, 2.0, 3.0, 3.5, 4.0, 4.5, and 4.9 mM CaCl₂ in ubiquitination
10 buffer, free Ca²⁺ concentrations were calculated to be 0.04, 0.1, 0.2, 0.4, 0.7, 1.4, and
11 6.7 μM, respectively.

12

13 ***In vitro* tubulation assay**

14 An *in vitro* tubulation assay was performed as described (Uezu *et al*, 2011; Tsujita *et al*,
15 2006) with slight modifications. Briefly, liposomes were prepared from brain lipids
16 (Folch lipids) supplemented with 1 % rhodamine-PE. The liposomes (0.2 mg/ml
17 liposomes) were incubated with the Nedd4L C2 domain (4.5 μM) or BAR domains (1.4
18 μM) at 25°C for 10 min in lipid buffer containing 3 mM CaCl₂ (0.3 μM Ca²⁺). The
19 sample was examined by fluorescence or electron microscopy. The tubulation assay
20 with mSA-αENaC-associated liposomes was performed using the sample mixture
21 utilized in the co-sedimentation assay in which mSA-αENaC-associated liposomes
22 (brain-lipid liposomes) were used.

23

1 **Negative-staining electron microscopy**

2 Negative-staining transmission electron microscopy was performed as described
3 (Shimada *et al*, 2007). Box and whisker plots were used to represent the distribution of
4 liposome diameters.

5

6 ***In vivo* ubiquitination assay**

7 HEK293 cells were used, because they formed membrane tubules upon FCHO2
8 expression more efficiently than did COS7 cells. HEK293 cells at approximately 90%
9 confluence on a 6-well plate were transfected with 0.8 µg of pCMV-Myc-Nedd4L, 1.6
10 µg of pEGFP-BAR domain, and 1.6 µg of pCGN-HA-Ub. In some experiments, cells
11 were transfected with various doses (0–1.5 µg) of pCMV-Myc-Nedd4L, 1.5 µg of
12 pEGFP-FCHO2 BAR domain, 1 µg of pCGN-HA-Ub, and 0.5 µg of pCAGI-Hygro-
13 FLAG-αENaC. Total transfected cDNA amount was held constant using empty pCMV-
14 Myc vector. Amiloride (40 µM) was added to the medium when αENaC cDNA was
15 transfected. At 21 h after transfection, cells were washed with PBS and incubated with
16 serum-free DMEM containing 1% BSA. After 3 h incubation, 10 µM MG132 was
17 added to the medium. After further 4 h incubation, cells were solubilized in 150 µl of
18 lysis buffer C (50 mM Tris-HCl at pH 7.5, 150 mM NaCl, 5 mM EDTA, 10 mM N-
19 ethylmaleimide, 1 mM PMSF, 10 µg/ml leupeptin, and 1 µg/ml pepstatin A) containing
20 1% SDS. After boiling, the sample was sonicated and then centrifuged at 20,000 × g for
21 15 min. The supernatant was diluted 10-fold with lysis buffer C containing 1% Triton
22 X-100 and then incubated at 4°C for 3 h with either anti-Myc or anti-FLAG M2
23 antibody. Protein G-Sepharose beads were added to the sample, which was then

1 incubated at 4°C for 3 h. After the beads were thoroughly washed with lysis buffer C
2 containing 1% Triton X-100, bound proteins were eluted by boiling in SDS sample
3 buffer for 5 min. These proteins were then subjected to SDS-PAGE, followed by IB.

4

5 ***In vitro* ubiquitination assay**

6 mSA- α ENaC-associated liposomes were made by incubating liposomes (10 μ g) with
7 mSA- α ENaC (35 pmol) in 25 μ l of lipid buffer, as described for the co-sedimentation
8 assay. They were then incubated at 25°C for 10 min with 0.07 μ M Nedd4L, 0.04 μ M E1
9 (Ube1), 0.7 μ M E2 (UbcH7), 7 μ M Ub, and various concentrations of BAR domains in
10 50 μ l of ubiquitination buffer containing 4 mM CaCl₂ (0.7 μ M Ca²⁺) and 2 mM ATP.
11 Where indicated, various concentrations of CaCl₂ were used. The ubiquitination
12 reaction was started by adding ATP and stopped by adding 10 μ l of 6 \times SDS sample.
13 The sample was then boiled, subjected to SDS-PAGE, and immunoblotted with anti-Ub
14 and anti- α ENaC antibodies. The chemiluminescence intensity was quantified by
15 scanning using ImageJ (NIH).

16

17 **Other procedures**

18 Stripping immunoblots for re-probing was carried out with the WB Stripping Solution
19 Strong (Nacalai Tesque) according to the manufacturer's protocol. Protein
20 concentrations were quantified with BSA as a reference protein by the Bradford method
21 (Bio-Rad) or the BCA method (Thermo Fisher Scientific). SDS-PAGE was performed
22 as described (Laemmli, 1970).

23

1 **Statistical analysis**

2 All experiments were performed at least three times (biological replication) and
3 representative results are shown. Data are shown as the mean \pm S.E.M. Student's tests,
4 one-way analysis of variance test, and two-way analysis of variance test were used to
5 evaluate statistical significances between different treatment groups.

6

7 **Data availability**

8 This study includes no data deposited in external repositories.

9

10 **Acknowledgments**

11

12 We thank Drs. H. Kai and M. Nakao for kindly providing us with ENaC and Ub
13 cDNAs, respectively. We are also grateful to Dr. T. Takenawa (Kobe University, Kobe,
14 Japan) for helpful discussions. This work was partly carried out at the Institute of
15 Molecular Embryology and Genetics, the Gene Technology Centre, and Research
16 Facilities of the School of Medicine, Kumamoto University. This study was supported
17 by JSPS KAKENHI Grant Numbers 19K06643 (to H.N.), 19K06544 (to Y.S.), and
18 Setsuro Fujii Memorial, The Osaka Foundation for Promotion of Fundamental Medical
19 Research (to Y.S.) and by grants from the Mochida Memorial Foundation, the Takeda
20 Science Foundation, and the Uehara Memorial Foundation (to K.K.).

21

22 **Disclosure and Competing Interests Statement**

23 The authors declare no competing interests.

1

2

1 **References**

2

- 3 Aguet F, Antonescu CN, Mettlen M, Schmid S & Danuser G (2013) Advances in
4 analysis of low signal-to-noise images link dynamin and AP2 to the function of an
5 endocytic checkpoint. *Dev Cell* 26: 279–291
- 6 Berndsen CE & Wolberger C (2011) A spectrophotometric assay for conjugation of
7 ubiquitin and ubiquitin-like proteins. *Anal Biochem* 418: 102–110
- 8 Butterworth MB (2010) Regulation of the epithelial sodium channel (ENaC) by
9 membrane trafficking. *Biochim Biophys Acta* 1802: 1166–77
- 10 Chang-Ileto B, Frere SG, Chan RB, Voronov SV, Roux A, & Di Paolo G (2011)
11 Synaptojanin 1-mediated PI(4,5)P₂ hydrolysis is modulated by membrane
12 curvature and facilitates membrane fission. *Dev. Cell* 20: 206–218
- 13 Doherty GJ & McMahon HT (2009) Mechanisms of endocytosis. *Annu Rev Biochem*
14 78: 857–902
- 15 Di Fiore PP, Polo S & Hofmann K (2003) When ubiquitin meets ubiquitin receptors: a
16 signalling connection. *Nat Rev Mol Cell Biol* 4: 491–497
- 17 Escobedo A, Gomes T, Aragon E, Martin-Malpartida P, Ruiz L, & Macias MJ (2014)
18 Structural basis of the activation and degradation mechaisms of the E3 ubiquitin
19 ligase Nedd4L. *Structure* 22: 1446–1457
- 20 Firsov D, Schild L, Gautschi I, Mérillat AM, Schneeberger E & Rossier BC (1996) Cell
21 surface expression of the epithelial Na channel and a mutant causing Liddle
22 syndrome: a quantitative approach. *Proc Natl Acad Sci U S A* 93: 15370–15375
- 23 Frost A, Perera R, Roux A, Spasov K, Destaing O, Egelman EH, De Camilli P & Unger

- 1 VM (2008) Structural basis of membrane invagination by F-BAR domains. *Cell*
2 132: 807–817
- 3 Henne WM, Boucrot E, Meinecke M, Evergren E, Vallis Y, Mittal R & McMahon HT
4 (2010) FCHo proteins are nucleators of clathrin-mediated endocytosis. *Science*
5 328: 1281–4
- 6 Henne WM, Kent HM, Ford MGJ, Hegde BG, Daumke O, Butler PJG, Mittal R,
7 Langen R, Evans PR & McMahon HT (2007) Structure and Analysis of FCHo2 F-
8 BAR Domain: A Dimerizing and Membrane Recruitment Module that Effects
9 Membrane Curvature. *Structure* 15: 839–852
- 10 Hershko A & Ciechanover A (1998) THE UBIQUITIN SYSTEM. *Annu Rev Biochem*
11 67: 425–479
- 12 Hughey RP, Mueller GM, Bruns JB, Kinlough CL, Poland PA, Harkleroad KL,
13 Carattino MD & Kleyman TR (2003) Maturation of the epithelial Na⁺ channel
14 involves proteolytic processing of the alpha- and gamma-subunits. *J Biol Chem*
15 278: 37073–37082
- 16 Hui E, Johnson CP, Yao J, Dunning FM & Chapman ER (2009) Synaptotagmin-
17 mediated bending of the target membrane is a critical step in Ca(2+)-regulated
18 fusion. *Cell* 138: 709–21
- 19 Ingham RJ, Gish G & Pawson T (2004) The Nedd4 family of E3 ubiquitin ligases:
20 functional diversity within a common modular architecture. *Oncogene* 23: 1972–
21 84
- 22 Laemmli UK (1970) Cleavage of structural proteins during the assembly of the head of
23 bacteriophage T4. *Nature* 227: 680–685

- 1 Lehmann M, Lukonin I, Noe F, Schmoranzer J, Clementi C, Loerke D & Haucke V
2 (2019) Nanoscale coupling of endocytic pit growth and stability. *Sci Adv* 5:
3 eaax5775
- 4 Lemmon M (2008) Membrane recognition by phospholipid-binding domains. *Nat Rev
5 Mol Cell Biol* 9: 99–111
- 6 Lim KH, Huang H, Pralle A & Park S (2013) Stable, high-affinity streptavidin
7 monomer for protein labeling and monovalent biotin detection. *Biotechnol Bioeng*
8 110: 57–67
- 9 Martens S, Kozlov MM & McMahon HT (2007) How synaptotagmin promotes
10 membrane fusion. *Science* 316: 1205–8
- 11 Miyahara M, Nakanishi H, Takahashi K, Satoh-Horikawa K, Tachibana K & Takai Y
12 (2000) Interaction of nectin with afadin is necessary for its clustering at cell-cell
13 contact sites but not for its cis dimerization or trans interaction. *J Biol Chem* 275:
14 613–618
- 15 Nishizuka Y (1992) Intracellular signaling by hydrolysis of phospholipids and
16 activation of protein kinase C. *Science* 258: 607–14
- 17 Peter BJ, Kent HM, Mills IG, Vallis Y, Butler PJG, Evans PR & McMahon HT (2004)
18 BAR domains as sensors of membrane curvature: the amphiphysin BAR structure.
19 *Science* 303: 495–9
- 20 Pickart CM & Raasi S (2005) Controlled synthesis of polyubiquitin chains. *Methods
21 Enzym* 399: 21–36
- 22 Roberts M, Barry S, Woods A, van der Sluijs P, & Norman J (2001) PDGF-regulated
23 rab4-dependent recycling of $\alpha\beta\gamma$ integrin from early endosomes is necessary for

- 1 cell adhesion and spreading. *Curr Biol* 11: 1392–1402
- 2 Rossier BC (2014) Epithelial sodium channel (ENaC) and the control of blood pressure.
- 3 *Curr Opin Pharmacol* 15: 33–46
- 4 Rotin D & Kumar S (2009) Physiological functions of the HECT family of ubiquitin
- 5 ligases. *Nat Rev Mol Cell Biol* 10: 398–409
- 6 Rotin D & Staub O (2011) Role of the ubiquitin system in regulating ion transport.
- 7 *Pflugers Arch* 461: 1–21
- 8 Saffarian S, Coccuci E, & Kirchhausen T (2009) Distinct dynamics of endocytic clathrin-
- 9 coated pits and coated palques. *PLoS Biol* 7: e1000191
- 10 Sakamoto Y, Kikuchi K, Umeda K & Nakanishi H (2017) Effects of various spacers
- 11 between biotin and the phospholipid headgroup on immobilization and
- 12 sedimentation of biotinylated phospholipid-containing liposomes facilitated by
- 13 avidin-biotin interactions. *J Biochem* 162: 221–226
- 14 Shaner NC, Lin MZ, McKeown MR, Steinbach PA, Hazelwood KL, Davidson MW &
- 15 Tsien RY (2008) Improving the photostability of bright monomeric orange and red
- 16 fluorescent proteins. *Nat Methods* 5: 545–551
- 17 Shimada A, Niwa H, Tsujita K, Suetsugu S, Nitta K, Hanawa-Suetsugu K, Akasaka R,
- 18 Nishino Y, Toyama M, Chen L, *et al* (2007) Curved EFC/F-BAR-domain dimers
- 19 are joined end to end into a filament for membrane invagination in endocytosis.
- 20 *Cell* 129: 761–772
- 21 Sugahara T, Koga T, Ueno-Shuto K, Shuto T, Watanabe E, Maekawa A, Kitamura K,
- 22 Tomita K, Mizuno A, Sato T, *et al* (2009) Calreticulin positively regulates the
- 23 expression and function of epithelial sodium channel. *Exp Cell Res* 315: 3294–

- 1 3300
- 2 Takano K, Toyooka K & Suetsugu S (2008) EFC/F-BAR proteins and the N-WASP–
3 WIP complex induce membrane curvature-dependent actin polymerization. *EMBO*
4 *J* 27: 2817–2828
- 5 Takei K, Slepnev VI, Haucke V & De Camilli P (1999) Functional partnership between
6 amphiphysin and dynamin in clathrin-mediated endocytosis. *Nat Cell Biol* 1: 33–
7 39
- 8 Traub LM (2009) Tickets to ride: selecting cargo for clathrin-regulated internalization.
9 *Nat Rev Mol Cell Biol* 10: 583–96
- 10 Tsujita K, Suetsugu S, Sasaki N, Furutani M, Oikawa T & Takenawa T (2006)
11 Coordination between the actin cytoskeleton and membrane deformation by a
12 novel membrane tubulation domain of PCH proteins is involved in endocytosis. *J*
13 *Cell Biol* 172: 269–279
- 14 Uezu A, Umeda K, Tsujita K, Suetsugu S, Takenawa T & Nakanishi H (2011)
15 Characterization of the EFC/F-BAR domain protein, FCHO2. *Genes Cells* 16:
16 868–878
- 17 Umeda K, Ikenouchi J, Katahira-Tayama S, Furuse K, Sasaki H, Nakayama M, Matsui
18 T, Tsukita S, Furuse M & Tsukita S (2006) ZO-1 and ZO-2 independently
19 determine where claudins are polymerized in tight-junction strand formation. *Cell*
20 126: 741–754
- 21 Wang J, Peng Q, Lin Q, Childress C, Carey D & Yang W (2010) Calcium activates
22 Nedd4 E3 ubiquitin ligases by releasing the C2 domain-mediated auto-inhibition. *J*
23 *Biol Chem* 285: 12279–12288

- 1 Wiesner S, Ogunjimi AA, Wang H-R, Rotin D, Sicheri F, Wrana JL & Forman-Kay JD
2 (2007) Autoinhibition of the HECT-type ubiquitin ligase Smurf2 through its C2
3 domain. *Cell* 130: 651–862
- 4 Yang B & Kumar S (2010) Nedd4 and Nedd4-2: closely related ubiquitin-protein
5 ligases with distinct physiological functions. *Cell Death Differ* 17: 68–77
- 6 Yin Y, Arkhipov A & Schulten K (2009) Simulations of Membrane Tubulation by
7 Lattices of Amphiphysin N-BAR Domains. *Structure* 17: 882–892
- 8 Zaccai N, Kadlecova Z, Dickson VK, Korobchevskaya K & Traub L (2022) FCHO
9 control AP2's initiating role in endocytosis through a Ptd-Ins(4,5)P2-dependent
10 switch. *Sci Adv* 8: eabn2018
- 11 Zhou R, Patel S V. & Snyder PM (2007) Nedd4-2 catalyzes ubiquitination and
12 degradation of cell surface ENaC. *J Biol Chem* 282: 20207–20212
- 13 Zhu K, Shan Z, Chen X, Cai Y, Cui L, Yao W, Wang Z, Shi P, Tian C, Lou J, *et al*
14 (2017) Allosteric auto-inhibition and activation of the Nedd4 family E3 ligase Itch.
15 *EMBO Rep* 18: 1618–1630
- 16
- 17
- 18

1 **Figure legends**

2

3 **Figure 1. FCHO2 is required for Nedd4L-mediated ubiquitination and endocytosis
4 of ENaC.**

5 A. Knockdown of FCHO2 or Nedd4L by siRNA. $\alpha\beta\gamma$ ENaC-HeLa cells treated with
6 each siRNA were analyzed by immunoblotting (IB).

7 B. Inhibition of ENaC endocytosis by knockdown of FCHO2 or Nedd4L. After cells
8 were transfected with each siRNA, cell-surface ENaC was labeled by incubating at 4°C
9 with anti-FLAG antibody. Endocytosis was started by incubating cells at 37°C for the
10 indicated periods of time and stopped by chilling cells on ice. Antibody bound to the
11 cell surface but not internalized was removed by acid stripping. After cells were
12 solubilized, the antibody-labeled internalized ENaC subunits were precipitated and
13 analyzed by IB (upper panel) and quantified (bottom and right panels). Internalization
14 was expressed as a percentage of the initial amount of cell-surface α ENaC determined
15 by lysing cells without incubation at 37°C or acid stripping. Data are shown as the mean
16 \pm S.E.M. of three independent experiments. **P < 0.01; ***P < 0.001 (Student's t-test).

17 C. Inhibition of transferrin receptor (TfR) endocytosis by FCHO2 knockdown. After
18 cells were transfected with each siRNA, cell-surface proteins were biotinylated at 4°C.
19 Cells were then incubated at 37°C for 10 min. Biotin was removed from the cell surface,
20 and internalized biotinylated proteins were precipitated with avidin beads. Samples
21 were subjected to IB with anti-TfR antibody and quantified. Internalization was
22 expressed as a proportion of the initial amount of TfR on the cell surface. Data are
23 shown as the mean \pm S.E.M. of three independent experiments. *P < 0.05 (Student's t-

1 test).

2 D. Restoration of α ENaC endocytosis by FCHO2 re-expression in knockdown cells.

3 After cells were transfected with the indicated siRNA and GFP construct, cell-surface

4 α ENaC was labeled with anti-FLAG antibody at 4°C. Cells were then incubated at 37°C

5 for 10 min. After acid stripping, cells were subjected to immunofluorescence

6 microscopy (left panels) and quantified (right panel). The antibody-labeled, internalized

7 α ENaC was visualized with a fluorescence-conjugated secondary antibody. The border

8 of each cell is delineated by a solid line. Arrows indicate cells expressing GFP-tagged

9 proteins. Scale bars, 10 μ m. The proportion of cells with internalized α ENaC among

10 cells expressing control GFP or GFP-siRNA-resistant (sr) -FCHO2 is shown. Data are

11 shown as the mean \pm S.E.M. of five independent images (31-71 cells expressing GFP-

12 tagged proteins per image). ***P < 0.001 (two-way analysis of variance with post hoc

13 test).

14 E, F. Effects of FCHO2, Nedd4L, and FBP17 knockdown on ENaC ubiquitination and

15 expression at the cell surface. After cells were transfected with each siRNA, cell-surface

16 α ENaC was biotinylated and sequentially precipitated with anti-FLAG antibody and

17 then avidin beads. Samples were subjected to IB with anti-FLAG and anti-Ub

18 antibodies (E) and quantified (F). E, ENaC ubiquitination, Asterisks indicate the same

19 band of ubiquitinated FLAG- α ENaC. F, ENaC expression at the cell surface. Data are

20 shown as the mean \pm S.E.M. of three independent experiments. *P < 0.05 (Student's t-

21 test).

22

23 **Figure 2. Localization of cell-surface ENaC, FCHO2, and Nedd4L at clathrin-
24 coated structures.**

1 A, B. Localization of cell-surface ENaC. mTagRFP-clathrin light chain (CLC) (A) or
2 Nedd4L C922A (catalytic inactive mutant)-GFP (B) was expressed in $\alpha\beta\gamma$ ENaC-HeLa
3 cells. Cell-surface α ENaC was labeled with anti-FLAG antibody at 4°C. Cells were then
4 fixed and stained with anti-FCHO2 antibody. Samples were subjected to
5 immunofluorescence microscopy (left panel). Insets represent enlarged images of the
6 dashed boxes. Scale bar, 10 μ m. Co-localization was analyzed (right panel). The mean
7 values of Pearson's correlation coefficient from three cells and the S.E.M. are shown. A.
8 Co-localization of cell-surface ENaC with FCHO2 at clathrin-coated structures. B. Co-
9 localization of cell-surface ENaC with Nedd4L C922A mutant and FCHO2.
10 C. Co-localization of Nedd4L with FCHO2 at clathrin-coated structures. Nedd4L-GFP
11 and mTagRFP-CLC were co-expressed in wild-type HeLa cells. Cells were then fixed
12 and stained with anti-FCHO2 antibody (left panel). Insets represent enlarged images of
13 the dashed boxes. **Scale bar, 10 μ m.** Co-localization was analyzed (right panel). The
14 mean values of Pearson's correlation coefficient from three cells and the S.E.M. are
15 shown.

16

17 **Figure 3. Recruitment of Nedd4L to CCPs.** DsRed-CLC were co-expressed with
18 Nedd4L-GFP in wild-type HeLa cells. Images were acquired at 1 s intervals through
19 TIRF microscopy. Upper panel, TIRF images of HeLa cells. Insets represent enlarged
20 images of the dashed boxes. Bottom panel, selected snapshots (every 10 sec) from a
21 time series were obtained from a single CCP indicated by the arrowhead. The time point
22 at which Nedd4L started to accumulate was set 0. Scale bar, 2 μ m.

23

24 **Figure 4. Recruitment of Nedd4L to membrane tubules generated by FCHO2 in**

1 **cells.**

2 GFP-BAR domains were co-expressed with Myc-Nedd4L proteins in COS7 cells (A)
3 and HEK293 cells (B). Cells were serum-starved and subjected to immunofluorescence
4 microscopy. Insets represent enlarged images of the dashed boxes. Scale bar, 10 μ m.

5

6 **Figure 5. Activation of Nedd4L by membrane tubules generated by FCHO2 in**
7 **cells.**

8 A–E. Nedd4L autoubiquitination. An *in vivo* ubiquitination assay was performed with
9 various BAR domains and FCHO2 mutants (A, B) and Nedd4L mutants (D). GFP-BAR
10 domains were co-expressed with Myc-Nedd4L proteins and HA-tagged Ub in HEK293
11 cells. Cell lysates were subjected to immunoprecipitation (IP) and analyzed by IB (A, B,
12 D). WT, wild type. Cells were also subjected to immunofluorescence microscopy (C, E).
13 Scale bar, 10 μ m.

14 F. α ENaC ubiquitination. An *in vivo* ubiquitination assay was performed with various
15 concentrations of Myc-Nedd4L using FALAG- α ENaC as a substrate in the presence or
16 absence of GFP-FCHO2 BAR domain. Cell lysates were subjected to IP. Samples were
17 analyzed by IB.

18

19 **Figure 6. The Nedd4L C2 domain is a Ca^{2+} -dependent PS binding domain.**

20 A co-sedimentation assay was performed with the C2 domain or full-length Nedd4L
21 using brain-lipid liposomes (~50% PS) at various Ca^{2+} concentrations (A) and with the
22 C2 domain using synthetic liposomes containing various percentages of PS at 0.3 μ M or
23 1.0 mM Ca^{2+} (B). The supernatants (S) and pellets (P) were subjected to sodium

1 dodecyl sulfate (SDS)-polyacrylamide gel electrophoresis (PAGE), followed by
2 Coomassie brilliant blue (CBB) staining (upper panels). Bottom panels, quantitative
3 analysis. (–) for $[Ca^{2+}]$ indicates EGTA alone. Data are shown as the mean \pm S.E.M. of
4 three independent experiments.

5 A. Ca^{2+} dependency.

6 B. PS dependency.

7

8 **Figure 7. Preference of Nedd4L for FCHO2-generated membrane curvature.**

9 A. Distribution of liposome diameters. Brain-lipid liposomes (~50% PS) of different
10 diameters were prepared by extrusion through the indicated pore sizes and sonication.

11 Left panel, electron microscopic images. Scale bars, 200 nm. Right panel, distribution
12 of liposome diameters shown by boxplots (number of observations per pore size = 25).

13 The center line inside the box corresponds to the median, the bounds of the box
14 encompass data points between the first and third quartiles, and the whiskers extend to
15 the minimum and maximum values including outliers. So, sonication.

16 B-D. Sensing and generation of membrane curvature by Nedd4L. Co-sedimentation (B)
17 and *in vitro* tubulation (C, D) assays were performed using brain-lipid liposomes (~50%
18 PS) at 0.1 μ M (B) and 0.3 μ M Ca^{2+} (C, D). B, Preference of Nedd4L for a specific
19 degree of membrane curvature. Liposomes were supplemented with X-biotin-PE and
20 rhodamine-PE. Full-length Nedd4L was incubated with liposomes of different sizes,
21 which were prepared by extrusion through the indicated pore sizes. The sample was
22 then incubated with avidin beads and ultracentrifuged. The proportion of precipitated
23 liposomes of each size was calculated to be ~100% by measuring both total and

1 supernatant fluorescence. The supernatants (S) and pellets (P) were subjected to SDS-
2 PAGE, followed by CBB staining (upper panel). Bottom panel, quantitative analysis.
3 So, sonication. Data are shown as the mean \pm S.E.M. of five independent experiments.
4 *P < 0.05; **P < 0.01 (one-way analysis of variance with Tukey's post hoc test). C,
5 Curvature generation by Nedd4L. The assay was performed with the Nedd4L C2
6 domain. Samples were examined by electron microscopy. Scale bar, 100 nm. D, The
7 degree of membrane curvature generated by Nedd4L is consistent with that generated
8 by FCHO2. The assay was performed with the indicated protein. Left panel, electron
9 microscopic image. Scale bar, 100 nm. Right panel, distribution of tubule diameters
10 shown by boxplots (number of observations per protein = 14–33). The center line inside
11 the box corresponds to the median, the bounds of the box encompass data points
12 between the first and third quartiles, and the whiskers extend to the minimum and
13 maximum values including outliers.

14

15 **Figure 8. Conserved hydrophobic residues of Nedd4L are responsible for sensing**
16 **and generation of membrane curvature.**

17 A. Sequence alignment of C2 domains. Conserved residues are highlighted with the
18 following color code: yellow, aspartates for Ca^{2+} binding; blue, very hydrophobic
19 residues probably for penetration into the lipid bilayer; and brown, others. Dots show
20 the mutation sites. Hs, *Homo sapiens*; Sc, *Saccharomyces cerevisiae*; and Rt, *Rattus*
21 *norvegicus*.

22 B. Inability of Nedd4L C2 domain mutants to sense membrane curvature in cells. GFP-
23 FCHO2 BAR domain and Myc-Nedd4L C2 domain mutants were co-expressed in

1 COS7 cells. Insets are enlarged images of dashed boxes. Scale bar, 10 μ m.
2 C, D. Inability of Nedd4L C2 domain mutants to bind to membranes and to generate
3 membrane curvature *in vitro*. Co-sedimentation (C) and *in vitro* tubulation (D) assays
4 were performed using brain-lipid liposomes (~50% PS) at 0.3 μ M Ca²⁺. C, Membrane
5 binding. The assay was performed with Nedd4L C2 domain mutants using various
6 concentrations of liposomes. The supernatants (S) and pellets (P) were subjected to
7 SDS-PAGE, followed by CBB staining (upper panel). Bottom panel, quantitative
8 analysis. Data are shown as the mean \pm S.E.M. of three independent experiments. D,
9 Curvature generation. The assay was performed with Nedd4L C2 domain mutants.
10 Samples were examined by fluorescence microscopy. Scale bar, 10 μ m.

11

12 **Figure 9. Properties of the catalytic activity and membrane binding of Nedd4L.**

13 Liposomes supplemented with biotinylated phospholipids were incubated with mSA-
14 α ENaC (A, B). Samples were mixed with Nedd4L. Mixtures were subjected to
15 ubiquitination (C-E) and co-sedimentation (F) assays. These assays were performed
16 with brain-lipid liposomes (~50% PS) at various Ca²⁺ concentrations (C), with synthetic
17 liposomes (various percentages of PS) at 0.7 μ M Ca²⁺ (D, F), and with brain-lipid
18 liposomes (20% PS) at 0.7 μ M Ca²⁺ (E). Ubiquitination and liposome binding were
19 quantified by scanning and expressed as ratios to maximum levels. Asterisks indicate
20 the same band of mono-ubiquitinated mSA- α ENaC.

21 A, B. Schematic diagrams of mSA- α ENaC. A, Structure. B. Binding to biotinylated
22 liposomes.

23 C. Ca²⁺-dependent Nedd4L activity. Ubiquitination was detected by IB (upper panel)

1 and the intensity was quantified by scanning (bottom panel). Data are shown as the
2 mean \pm S.E.M. of three independent experiments.

3 D, Membrane localization of mSA- α ENaC enhances the PS-dependent catalytic activity
4 of Nedd4L. Assays were performed in the presence or absence of 40 μ M biotin.
5 Ubiquitination was detected by IB (left panel). The intensities were quantified by
6 scanning (right panel). Data are shown as the mean \pm S.E.M. of three independent
7 experiments.

8 E, Nedd4L activity is predominantly stimulated by the specific degree of membrane
9 curvature. The assay was performed using liposomes of different sizes which were
10 prepared by extrusion through the indicated pore sizes. Ubiquitination was detected by
11 IB (left panel) and quantified (right panel). Data are shown as the mean \pm S.E.M. of
12 three independent experiments. ***P < 0.001 (one-way analysis of variance with
13 Tukey's post hoc test).

14 F, Membrane localization of mSA- α ENaC enhances the PS-dependent membrane
15 binding of Nedd4L. Assays were performed in the presence or absence of 40 μ M biotin.
16 Liposome binding was detected by IB (left panel). The intensities were quantified by
17 scanning (right panel). T, total sample. P, pellet. Data are shown as the mean \pm S.E.M.
18 of three independent experiments.

19

20

21 **Figure 10. Recruitment and activation of Nedd4L by FCHO2-generated membrane
22 curvature *in vitro*.**

23 mSA- α ENaC-associated brain-lipid liposomes (20% PS) were mixed with Nedd4L in

1 the presence or absence of BAR domains. Mixtures were subjected to co-sedimentation
2 (A) and ubiquitination (B-E) assays. These assays were performed at 0.7 μ M Ca²⁺ with
3 brain-lipid liposomes (20%PS) (A, B, D, and E) and with the indicated (20% PS or
4 ~50% PS) brain-lipid liposomes (C). Ubiquitination and liposome binding were
5 quantified by scanning and expressed as ratios to maximum levels. Asterisks indicate
6 the same band of mono-ubiquitinated mSA- α ENaC.

7 A. FCHO2-induced recruitment of Nedd4L. The assay was performed with the FCHO2
8 BAR domain (1.4 μ M, 50 μ g/ml) in the presence or absence of biotin. The total sample
9 (T) and pellets (P) were subjected to SDS-PAGE, followed by CBB staining (FCHO2
10 BAR) and IB (Nedd4L and mSA- α ENaC).

11 B, C. FCHO2-induced activation of Nedd4L. B, Effects of various doses of the FCHO2
12 BAR domain. The assay was performed with various concentrations of the FCHO2
13 BAR domain. Ubiquitination was detected by IB (left panel) and the intensity was
14 quantified by scanning (right panel). C, Effects of the PS percentage in liposomes. The
15 assay was performed with the FCHO2 BAR domain (1.4 μ M). Samples were analyzed
16 by IB. Data are shown as the mean \pm S.E.M. of three independent experiments.

17 D, E. Specificity of BAR domains and effect of an FCHO2 mutant. The assay was
18 performed with various BAR domains (D) and an FCHO2 mutant (E) (1.4 μ M each).
19 Samples were analyzed by IB.

20

21 **Figure 11. Effects of PI(4,5)P₂ on FCHO2-induced recruitment and activation of**
22 **Nedd4L.**

23 A, B. Binding to PI(4,5)P₂. A co-sedimentation assay was performed at 0.7 μ M Ca²⁺

1 with the FCHO2 BAR or Nedd4L C2 domain using mSA- α ENaC-associated synthetic
2 liposomes containing 20% PS, 5% PI(4,5)P₂ (A), or various percentages of PI(4,5)P₂
3 (B). The supernatants (S) and pellets (P) were subjected to SDS-PAGE, followed by
4 CBB staining (A and upper panel in B). Bottom panel in B, quantitative analysis.
5 Control, synthetic liposomes [0% PS and 0% PI(4,5)P₂]. Data are shown as the mean \pm
6 S.E.M. of three independent experiments.

7 C, D. Effects on FCHO2-induced recruitment and activation of Nedd4L. Co-
8 sedimentation (C) and ubiquitination (D) assays were performed at 0.7 μ M Ca²⁺ with
9 mSA- α ENaC-associated synthetic liposomes containing 20% PS or 5% PI(4,5)P₂ in the
10 presence or absence of the FCHO2 BAR domain. C, Nedd4L recruitment. The total
11 sample (T) and pellets (P) were subjected to SDS-PAGE, followed by IB with anti-
12 Nedd4L antibody (upper panel) and CBB staining (lower panel). D, Nedd4L activation.
13 Samples were analyzed by IB. Asterisks indicate the same band of mono-ubiquitinated
14 mSA- α ENaC.

15

16 **Figure 12. Effects of liposome size on FCHO2-induced activation of Nedd4L.** Co-
17 sedimentation (A) and ubiquitination (B) assays were performed at 0.7 μ M Ca²⁺ with
18 the FCHO2 BAR domain using brain-lipid liposomes (20% PS, 0.8 μ m or 0.05 μ m
19 pore-size) that were associated with mSA- α ENaC.

20 A. Binding of the FCHO2 BAR domain to 0.8 μ m and 0.05 μ m pore-size liposomes.
21 The co-sedimentation assay was performed using synthetic (0% PS) or brain-lipid
22 liposomes (20% PS) containing rhodamine-PE and fluorescein-PE. Liposomes were
23 precipitated with anti-fluorescein antibody. The total sample (T) and pellets (P) were

1 subjected to SDS-PAGE, followed by CBB staining. The proportion of precipitated
2 liposomes of each size was calculated to be ~100% by measuring both total and
3 supernatant fluorescence.

4 B. Effects of liposome size on FCHO2-induced activation of Nedd4L. Samples were
5 analyzed by IB. Asterisks indicate the same band of mono-ubiquitinated mSA- α ENaC.

6

7 **Figure 13. Model of ENaC endocytosis.**

8 FCHO2 binds to the plasma membrane and generates a specific degree of membrane
9 curvature according to the intrinsic curvature of its BAR domain. Nedd4L exists in a
10 catalytically autoinhibited state due to an intramolecular interaction between the N-
11 terminal C2 and C-terminal HECT domains. Nedd4L is recruited to FCHO2-generated
12 membrane curvature at the rim of nascent CCPs that ENaC enters. Membrane binding
13 of the C2 domain causes catalytic activation by relieving autoinhibition. ENaC is
14 ubiquitinated and captured by adaptor proteins with Ub-interacting motifs, such as
15 Eps15.

16

17 **Extended View Figure Legends**

18

19 **Figure EV1. Expression of ENaC subunits in $\alpha\beta\gamma$ ENaC-HeLa cells.**

20 A, B. Doxycycline (Dox)-induced expression of α ENaC. $\alpha\beta\gamma$ ENaC-HeLa cells were
21 cultured overnight in the presence or absence of Dox. The lysates of parental HeLa and
22 $\alpha\beta\gamma$ ENaC-HeLa cells were subjected to IB. A, 7.5% gel. B, Gradient gel (5-20%). Anti-
23 γ ENaC antibody cross-reacted with two bands of endogenous proteins in parental HeLa

1 cells, the lower band of which overlapped with γ ENaC (arrow) in $\alpha\beta\gamma$ ENaC-HeLa cells.
2 Upon Dox-induced α ENaC expression, an additional 70-kDa γ ENaC band (asterisk)
3 was detected. It has been shown that co-expression of all three subunits induces ENaC
4 maturation, including proteolytic cleavage of α - and γ ENaC (Hughey *et al*, 2003). The
5 70-kDa γ ENaC band is likely a cleavage product comprising the C-terminal region. The
6 20-kDa α ENaC band (arrowhead) is likely a cleavage product comprising the N-
7 terminal region.

8 C. Association of α -, β -, and γ ENaC. When α ENaC was immunoprecipitated with anti-
9 FLAG antibody from $\alpha\beta\gamma$ ENaC-HeLa cells treated with Dox, β - and γ ENaC were co-
10 precipitated. **Asterisk, 70-kDa γ ENaC band.**

11

12 **Figure EV2. Knockdown of FBP17 by siRNA.**

13 $\alpha\beta\gamma$ ENaC-HeLa cells were treated with each siRNA, and FBP17 mRNA levels were
14 quantified using real-time PCR. The expression of FBP17 was normalized to GAPDH
15 mRNA levels. Data are shown as the mean \pm S.E.M. of three independent experiments.
16 ***P < 0.001 (Student's t-test).

17

18 **Figure EV3. Inability of FCHO2 mutants to generate membrane tubules.**

19 GFP-FCHO2 BAR domain [wild type (WT) or mutant] was expressed in COS7 cells.
20 Cells were then subjected to immunofluorescence microscopy. Scale bar, 10 μ m.

21

22 **Figure EV4. Inability of Nedd4L mutants to ubiquitinate α ENaC.** An *in vivo*
23 ubiquitination assay was performed with various Nedd4L constructs (each 0.5 μ g) using

1 FLAG- α ENaC as a substrate in the presence or absence of GFP-FCHO2 BAR domain.
2 Cell lysates were subjected to IP. Samples were analyzed by IB.

3

4 **Figure EV5. Inhibition of the liposome binding of Nedd4L by the FCHO2 BAR**
5 **domain.**

6 A co-sedimentation assay was performed at 0.7 μ M Ca^{2+} with control liposomes (0%
7 PS) or brain-lipid liposomes (~50% PS) in the presence or absence of the FCHO2 BAR
8 domain. The total sample (T) and pellets (P) were subjected to SDS-PAGE, followed by
9 IB (upper panel) and CBB staining (lower panel).

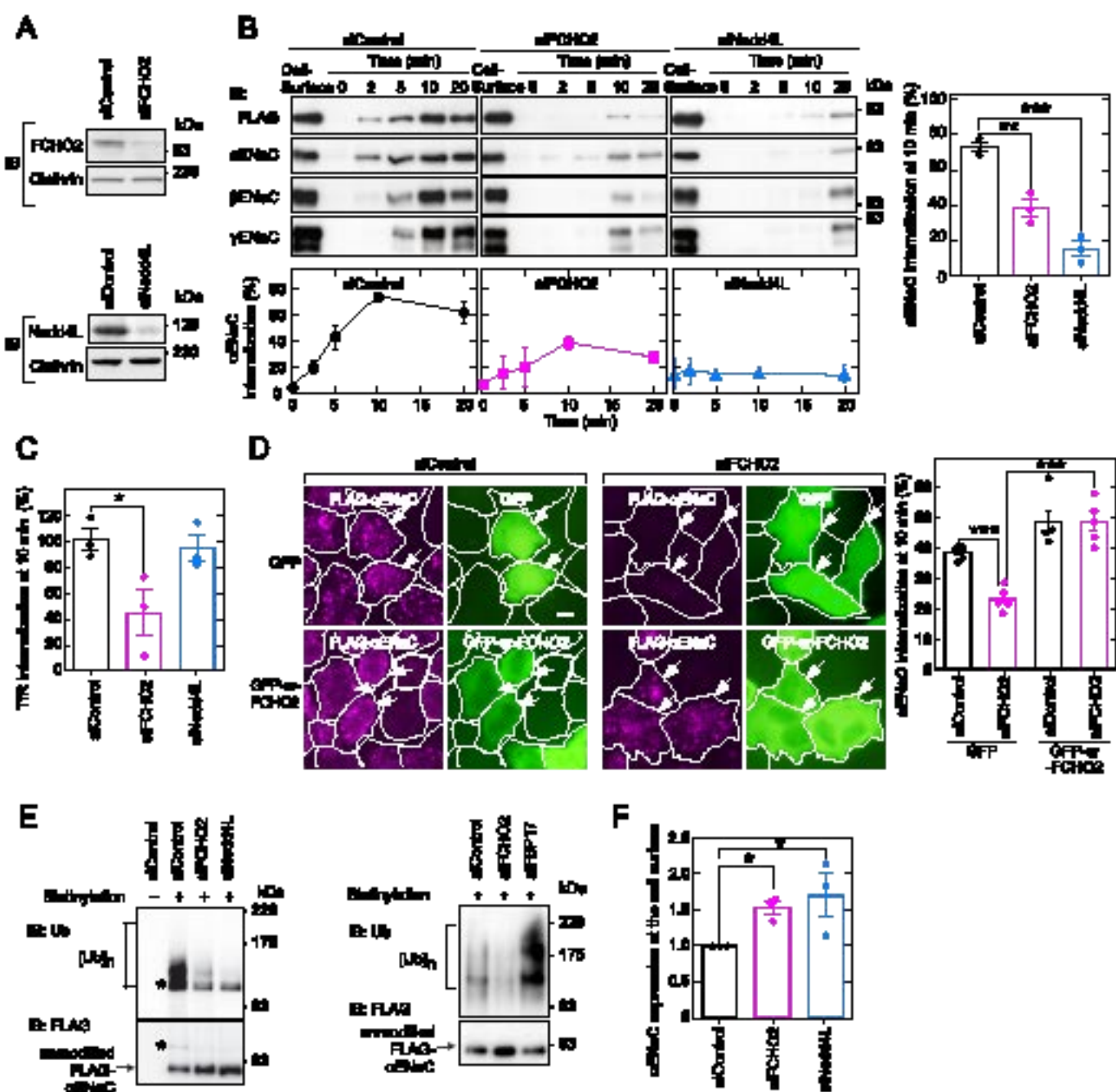
10

11 **Figure EV6. Membrane binding and curvature generation of BAR domains and an**
12 **FCHO2 mutant.** Co-sedimentation (A) and *in vitro* tubulation (B) assays were
13 performed at 0.7 μ M Ca^{2+} with the indicated BAR domains using brain-lipid liposomes
14 (20% PS) that were associated with mSA- α ENaC.

15 A. Membrane binding. The supernatants (S) and pellets (P) were subjected to SDS-
16 PAGE followed by CBB staining.

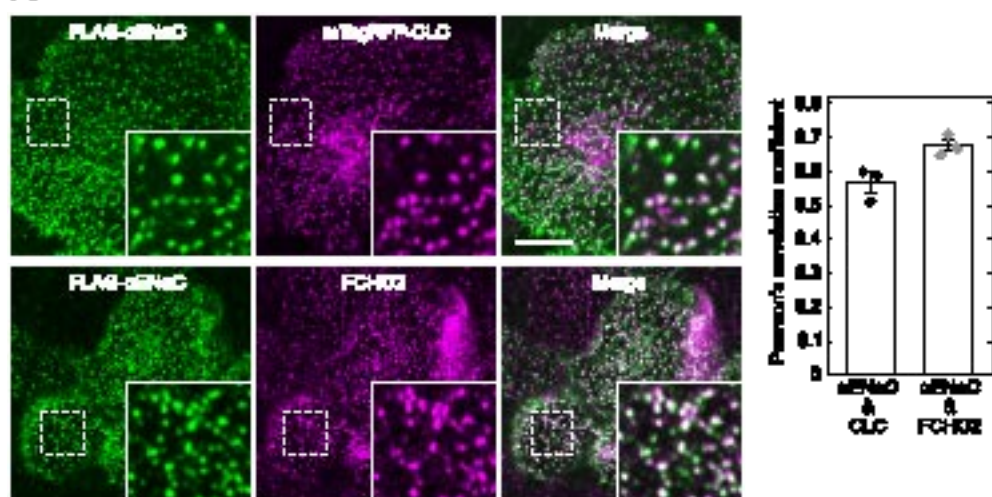
17 B. Curvature generation. Left panel, electron microscopic image. Scale bar, 100 nm.
18 Right panel, distribution of tubule diameters shown by boxplots (number of
19 observations per protein = 22–26). The center line inside the box corresponds to the
20 median, the bounds of the box encompass data points between the first and third
21 quartiles, and the whiskers extend to the minimum and maximum values including
22 outliers.

Sakamoto et al., Figure 1

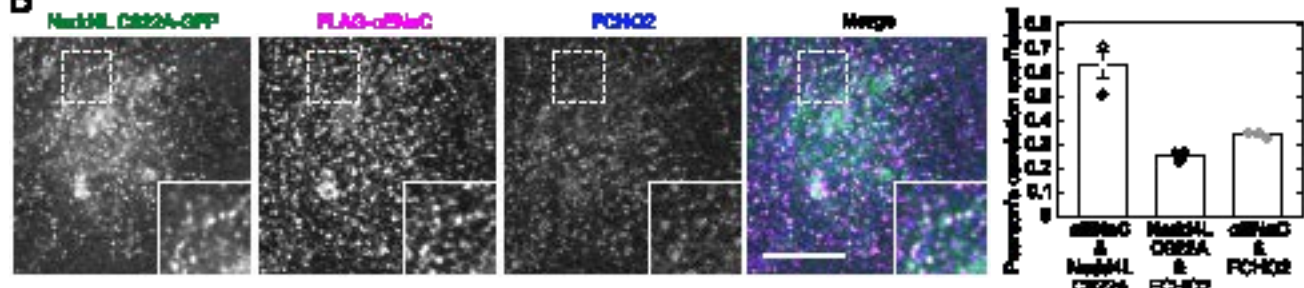


Sakamoto et al., Figure 2

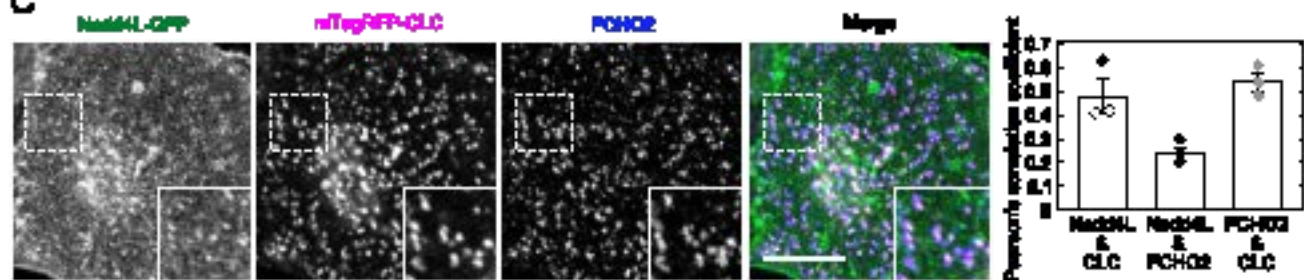
A



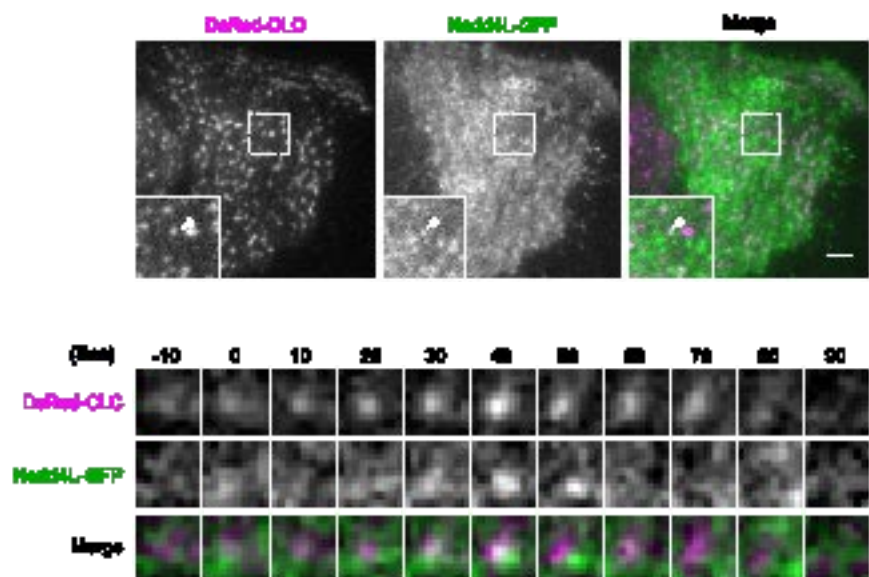
B



C

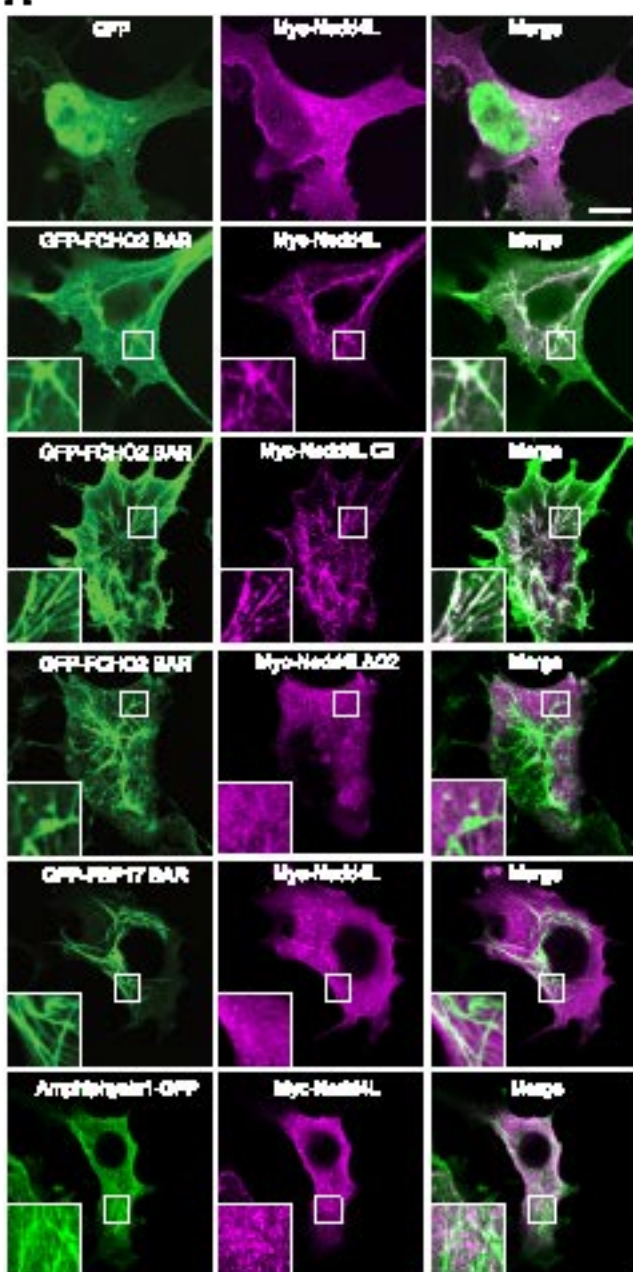


Sakamoto et al., Figure 3

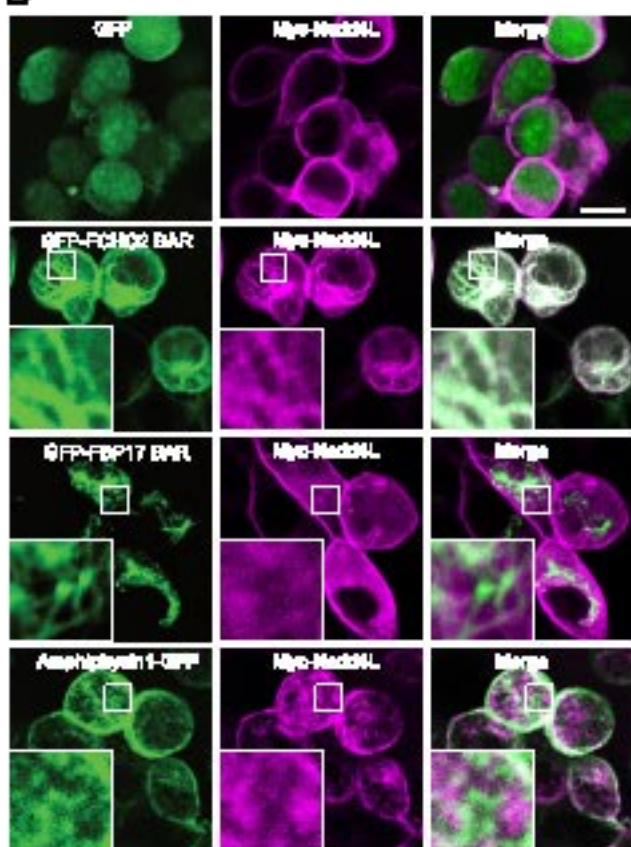


Sakamoto et al., Figure 4

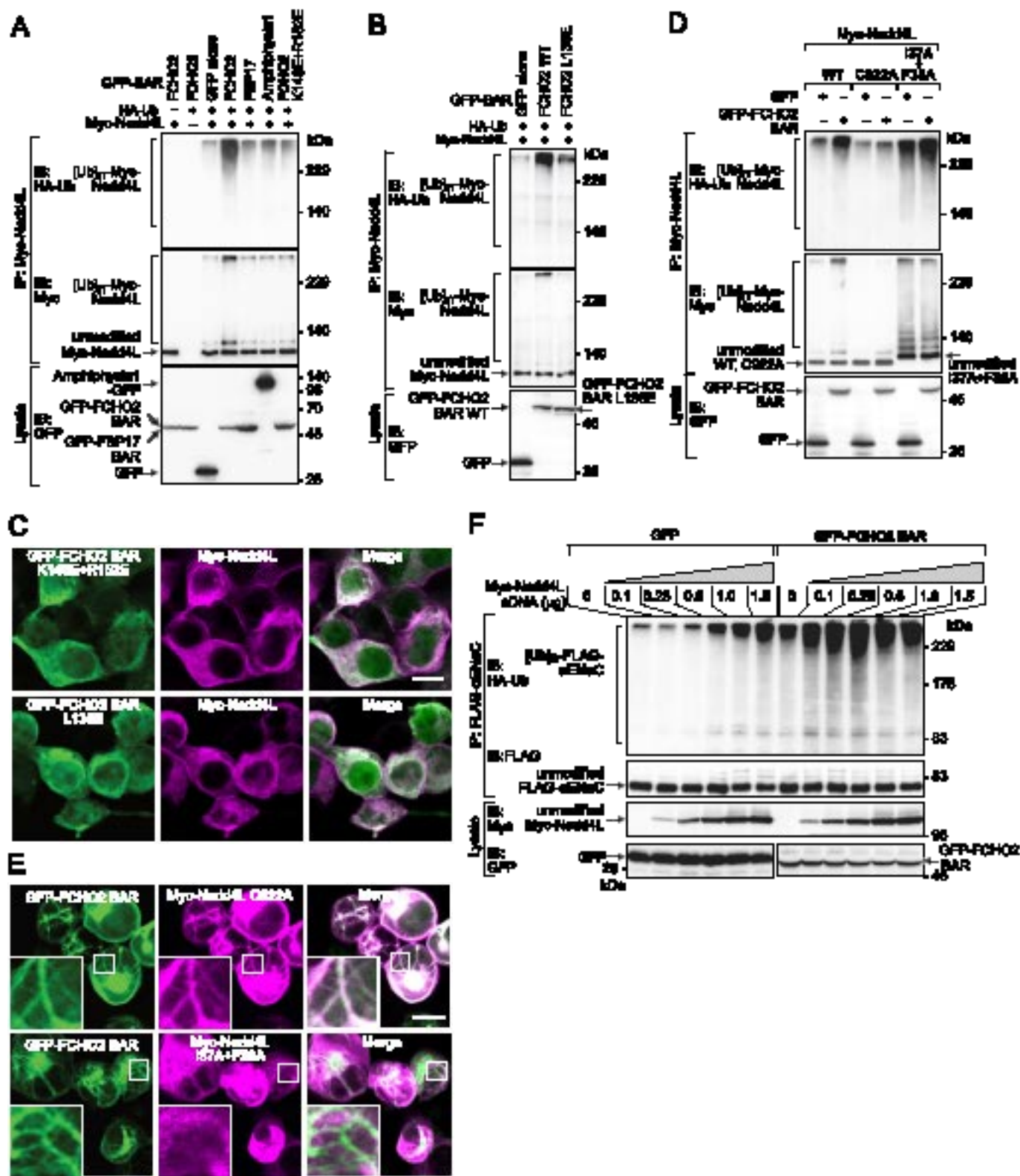
A



B

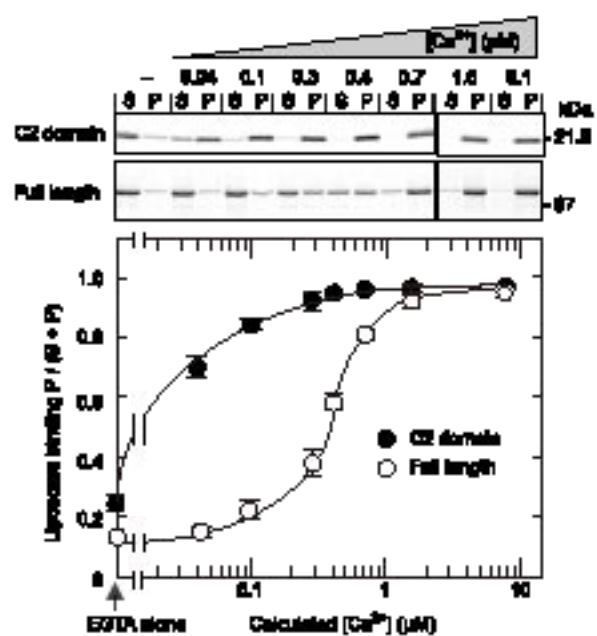


Sakamoto et al., Figure 5

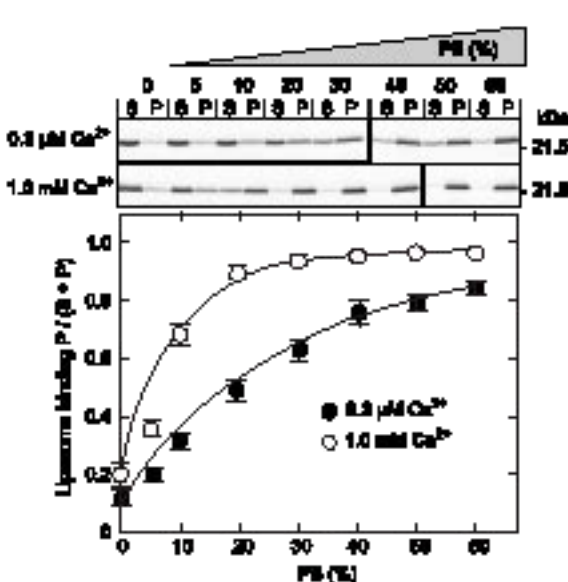


Sakamoto et al., Figure 6

A

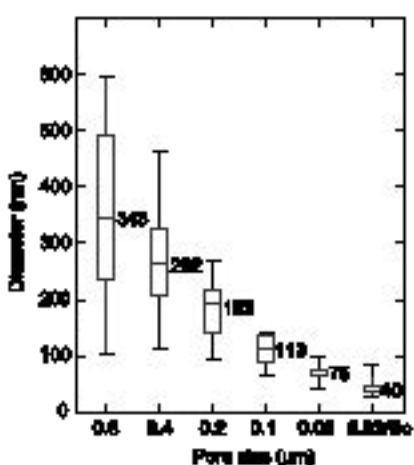
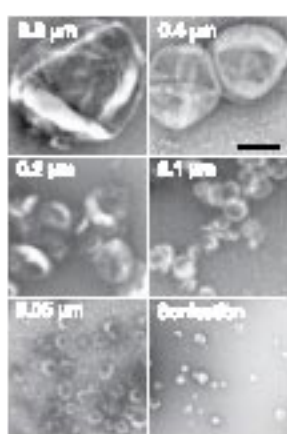


B

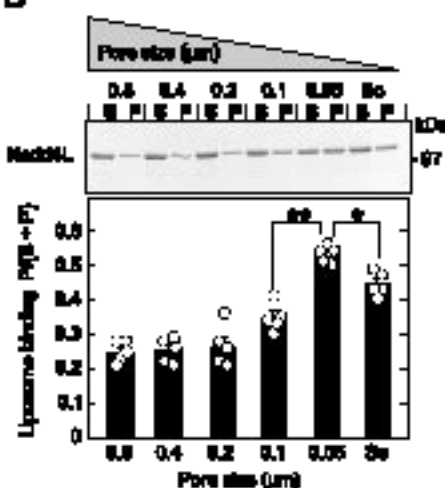


Sakamoto et al., Figure 7

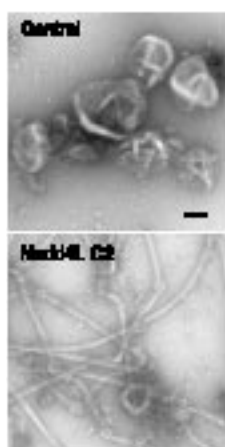
A



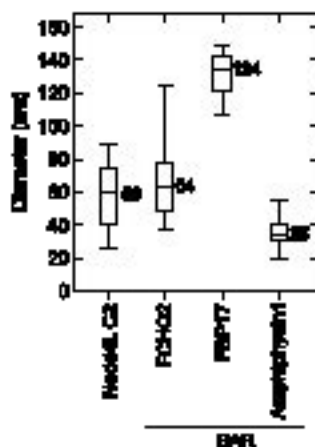
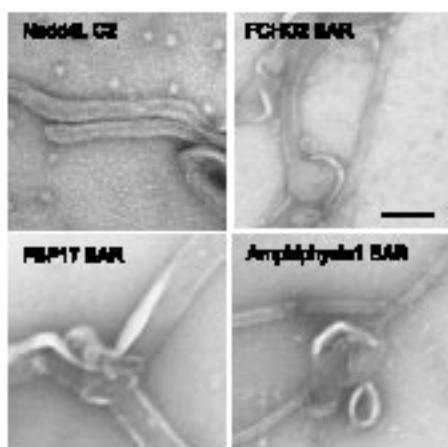
B



C

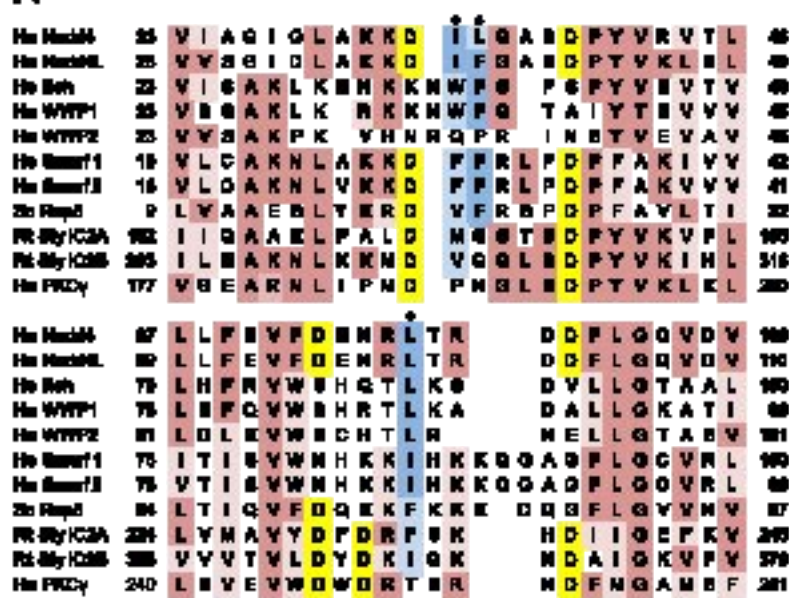


D

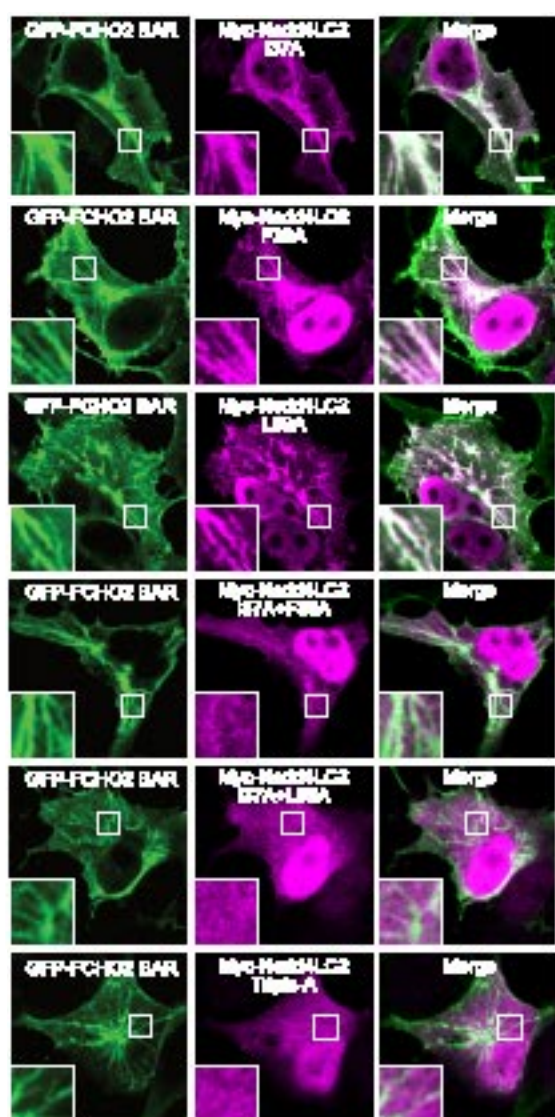


Sakamoto et al., Figure 8

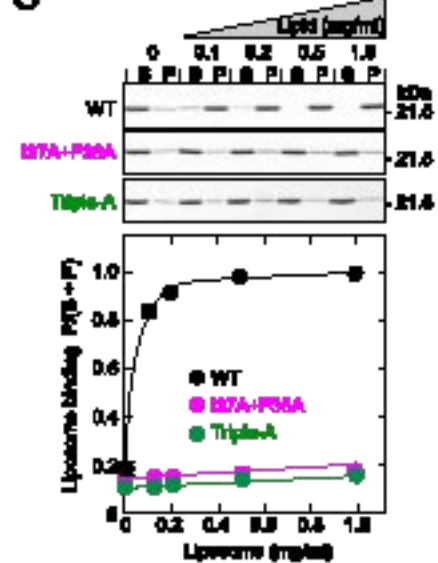
A



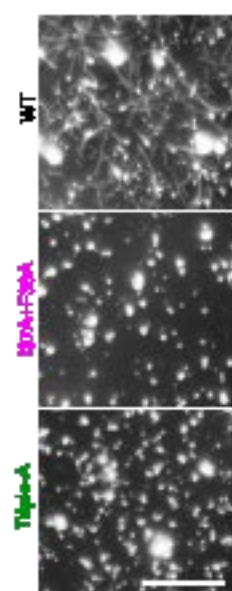
B



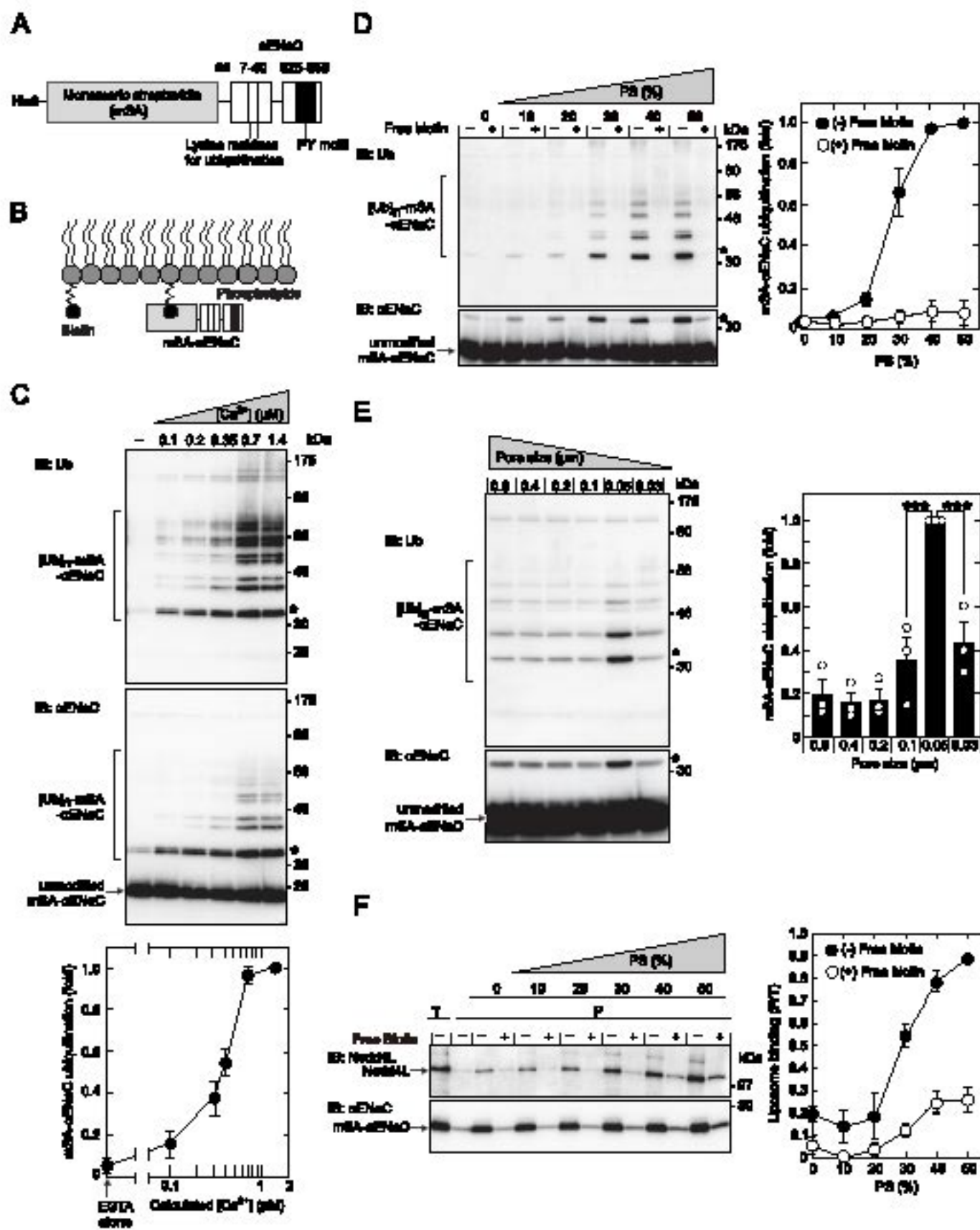
C



D

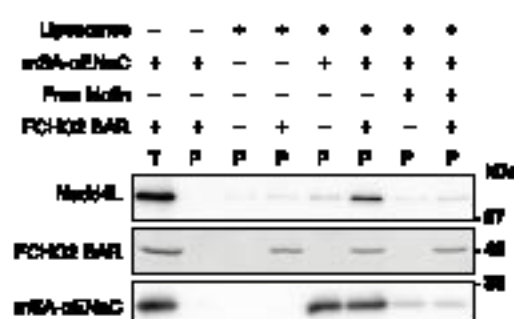


Sakamoto et al., Figure 9

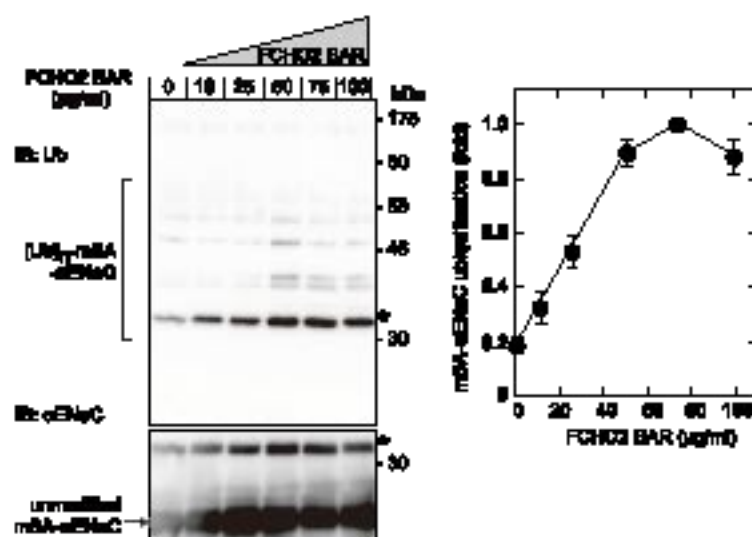


Sakamoto et al., Figure 10

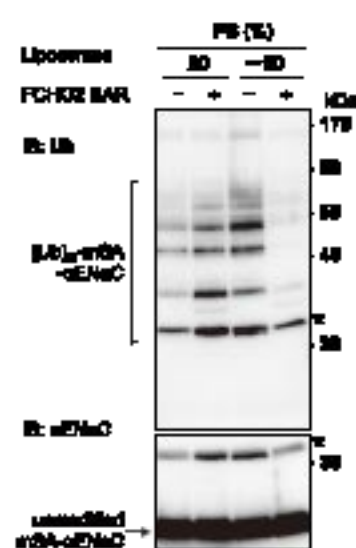
A



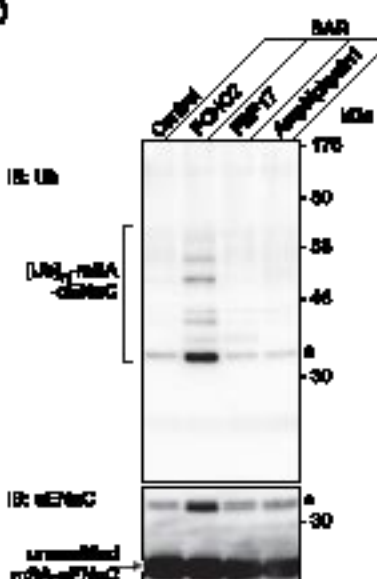
B



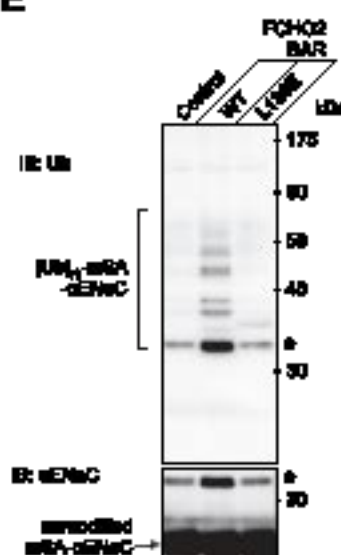
C



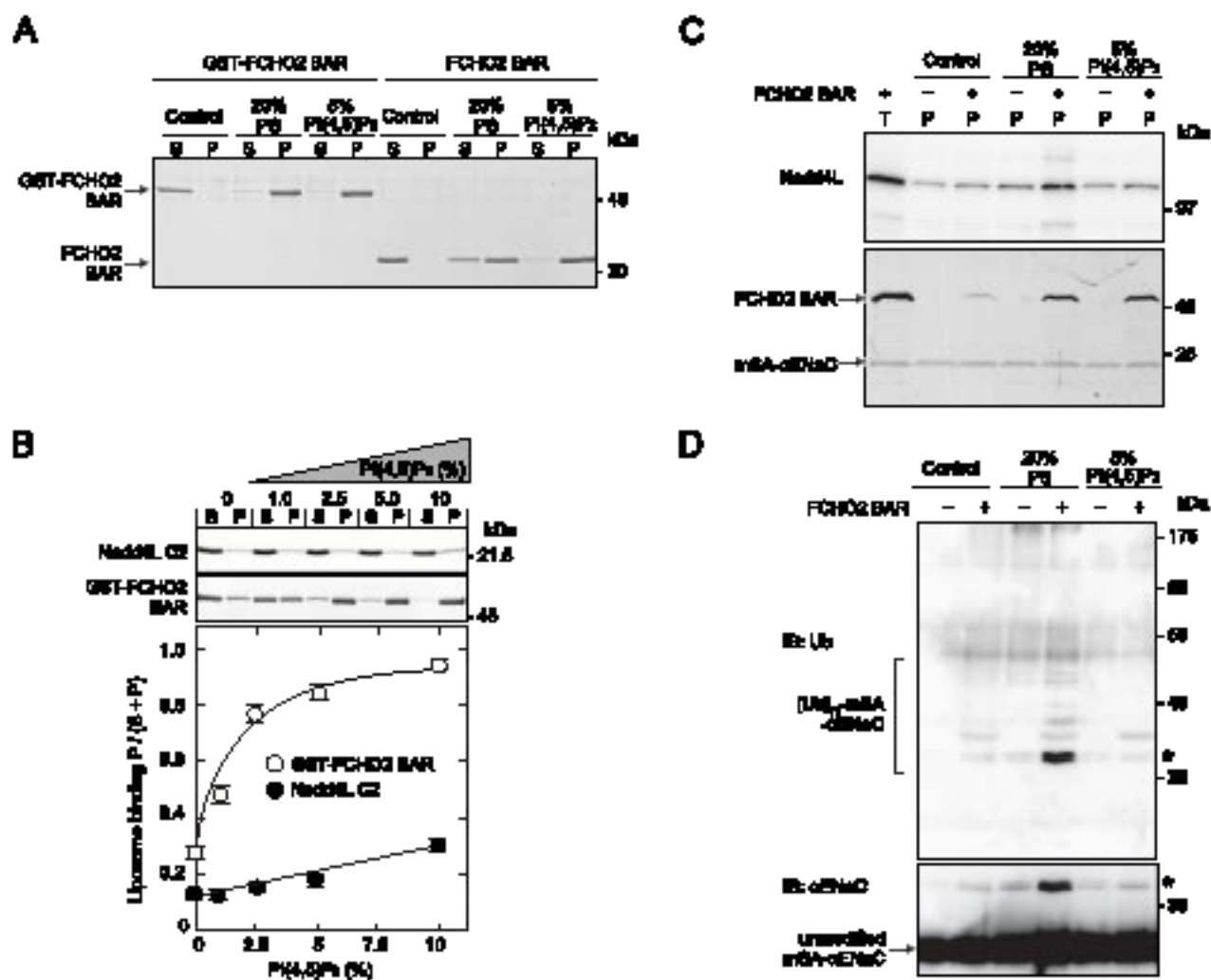
D



E

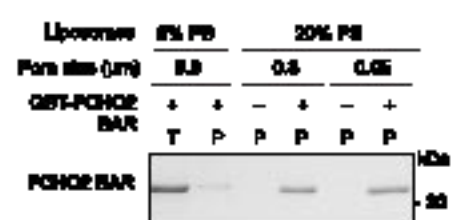


Sakamoto et al., Figure 11

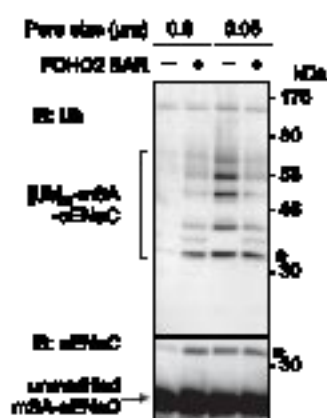


Sakamoto et al., Figure 12

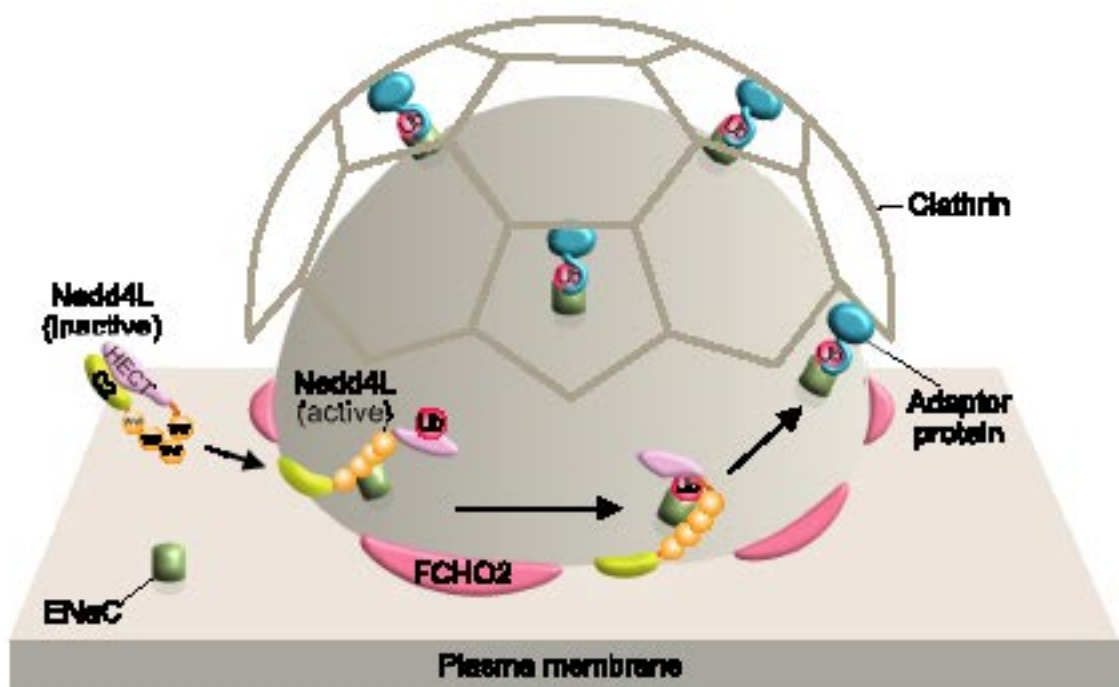
A



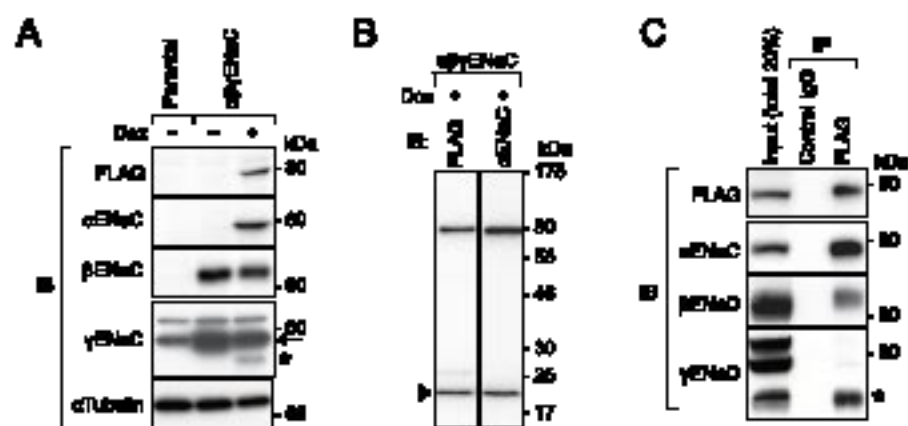
B



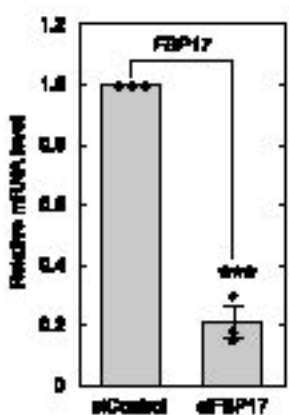
Sakamoto et al., Figure 13



Sakamoto et al., Figure EV1



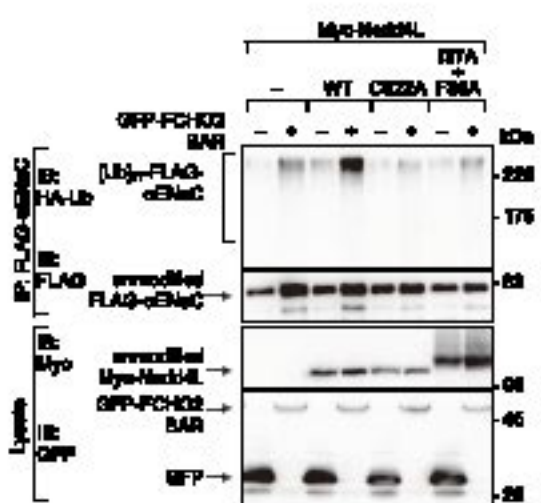
Sakamoto et al., Figure EV2



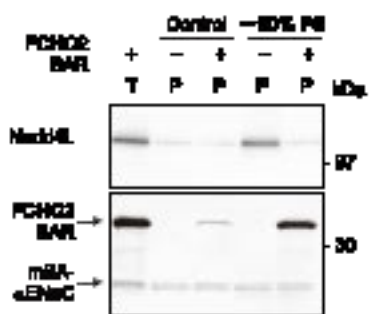
Sakamoto et al., Figure EV3



Sakamoto et al., Figure EV4



Sakamoto et al., Figure EV5



Sakamoto et al., Figure EV6

